UAH Research Report No. 146 May 1973

THERMAL ENGINEERING RESEARCH

(NASA-CR-124481) THERMAL ENGINEERING RESEARCH Final Report (Alabama Univ., Huntsville.) 93 p HC $6.75 CSCL 20K N74-12569

G3/33 Unclas 15469

Final Report

This research work was supported by
The NASA/MSFC
Under UAH-MSFC/NASA Cooperative Agreement Modification No. 1

The University of Alabama in Huntsville
Huntsville, Alabama

UAH Reseach Report No. 146 May 1973

THERMAL ENGINEERING RESEARCH

Final Report

This research work was supported by
The NASA/MSFC
Under UAH-MSFC/NASA Cooperative Agreement Modification No. 1

The University of Alabama in Huntsville
Huntsville, Alabama

PREFACE

This final report of efforts for the UAH-MSFC/NASA Cooperative Agreement Modification No. 1 (Thermal Engineering Research) presents the results of the following projects for the period from September 1971 through May 1973:

PROJECT I Analytical Treatment of Gas Flows Through Multilayer Insulation

PROJECT II Study of Deposition Model of Frost and Ice From Humid Gas in Ducts

PROJECT III Analysis of Thermal Environment in the Thrustor Cavity of Space Vehicles

Due to the diversity of the projects' requirements, the projects were assigned to three teams of research personnel. Under the general supervision of the Principal Investigator, the responsibility of technical direction for Project I was assigned to J. T. Lin; Project II was originally assigned to R. W. Blanton, and subsequently to C. C. Shih; Project III was assigned to J. J. Brainerd. Project I was carried out solely by J. T. Lin with minor assistance from the F&TE Lab staff. The bulk of work for Project II was carried out by B. K. Singh, then Bhuminder Singh. Project III was conducted mainly by Jim Chiou under proper technical guidance.

To make the success of this study possible valuable assistance was provided by the following staff members of the Fluid Dynamics Laboratory at the F&TE Laboratory of The University of Alabama in Huntsville:

Margaret P. Cuthill	Carol Holladay	Debbie Maples
Tommie McMeans	Don Miller	Barbra Oedamer
Thomas A. White	and other undergraduate lab assistants.	

The computer laboratory, instrumentation laboratory, and machine shop of The University of Alabama in Huntsville also provided useful assistance to the projects.

Cornelius C. Shih
Principal Investigator

UAH-MSFC/NASA Cooperative Agreement

Modification No. 1

Project I

Analytical Treatment of Gas Flows Through Multilayer Insulation

Final Report

by

J. T. Lin

Department of Fluid & Thermal Engineering
School of Graduate Studies and Research
The University of Alabama in Huntsville
P. O. Box 1247
Huntsville, Alabama 35807

ABSTRACT

A theoretical investigation of gas flow inside a multilayer insulation system has been made for the case of the broadside pumping process. A set of simultaneous first-order differential equations for the temperature and pressure of the gas mixture was obtained by considering the diffusion mechanism of the gas molecules through the perforations on the insulation layers. A modified Runge-Kutta method was used for numerical experiment. The numerical stability problem was investigated. It has been shown that when the relaxation time is small compared with the time period over which the gas properties change appreciably, the set of differential equations can be replaced by a set of algebraic equations for solution. Numerical examples were given, and comparisons with experimental data were made.

Nomenclature

A	area of one insulation layer (one side)
a	total area of perforation on one insulation layer
a'	$a' = (1 - c)A$
c	perforation coefficient $c = a/A$
k	Boltzmann constant
l	number of interstitial spaces between insulation layers
M	number of kinds of absorbed gases plus 1
m	mass of a gas molecule or an integer
N	number of gas molecules
n	number density of gas molecules or an integer
p	pressure
Q, q, R	outgassing rates, see Equations (4), (7), and (12)
T	temperature
t	time
V	volume
v	mean thermal velocity of gas molecules
δ	number of degrees of freedom of a gas molecule
τ	relaxation time
Subscripts:	subscript c refers to quantities inside the vacuum chamber; f to condition of the fuel tank; a to atmospheric condition; other subscripts refer to quantities in a certain interstitial space
Superscripts:	superscript 1 refers to the purge gas, other superscripts refer to a certain kind of gas molecules

1. Introduction

Recent developments in propulsion technology have stimulated interest in the study of multilayer insulation systems** for the fuel tank of a rocket booster. The purpose of multilayer insulations is to eliminate heat conduction between the fuel tank and the environment. It is then desirable that the spaces between the insulation layers be maintained at low pressures. However, it is not practical to require complete vacuum in the spaces between the insulation layers, although it would be ideal in principle, for the reasons that, complete vacuum is hardly attainable, and that when the pressure gets too low, deformation of the layers would cause solid contacts, which in turn would induce heat conduction. It is therefore customary in practice to require a pressure to be of the order of 10^{-4} torr. This low pressure is usually achieved before launch from the ambient pressure by some pumping device. There have been two pumping procedures in practice; namely, the broadside pumping by which the direction of gas flow is perpendicular to the insulation layers, and the edge pumping which causes the gas to flow parallel to the layers. Experiments of both evacuation procedures have been performed and results reported.[1,2,3] The present work is a theoretical analysis for the broadside pumping process.

In the case of broadside pumping, the insulation layers are perforated so that gas molecules can go through small holes on the layers, resulting in streaming gas motion perpendicular to the insulation layers. It is obvious that, in order to minimize layer deformation and solid contacts, small pressure differentials across the layers should be maintained during evacuation. This can be achieved by small perforation, i.e., the total area of the holes on an insulation layer is small compared to the total area of that layer. If we further require that the diameter of a single hole be small or comparable to the distance between two successive layers, there is the advantage of uniformity of gas motion, which renders convenience during operation.

** A multilayer insulation system consists of a large number, (in the order of 10^2) of extremely thin sheets of low thermal conductivity and lightweight materials, kept parallel to one another with a total thickness of about 1".

2. Formulation

Consider a fuel tank of simple geometry wrapped with multilayer insulation and situated inside a vacuum chamber. Consider the broadside pumping process and assume that the perforation areas are small. Then, a gas molecule in any interstitial space between two successive layers will, on the average, collide many times with the walls or with some other gas molecules in that interstice before getting through a hole to a neighboring interstice. Thus, it is plaussible to assume that the gas in any interstitial space is in thermal equilibrium with the temperature and pressure pertinent to that interstice, and the motion of the gas is simply a diffusion process.

Consider the gas inside the insulation system as a mixture of a certain kind of purge gas and a number of different kinds of gases originally absorbed in the insulation materials. Let A_1 be the total area of the outermost insulation layer (one side), and c_1 the perforation coefficient of the same layer (the ratio of the total perforation area on the first layer to A_1), and so on. Let V_1 be the volume of the interstice between the first and the second insulation layers, and N_1 the number of molecules in V_1. V_2 the volume of the interstice between the second and the third insulation layers, and N_2 the number of molecules in V_2, and so on. Since the gases in any interstice are in thermal equilibrium, each component gas has a Maxwellian distribution with its local density and the common local temperature. From the kinetic theory of gases, we have, for the gases in the i th interstice,

$$\frac{dN_i^{(j)}}{dt} = \frac{a_i}{4}\left(n_{i-1}^{(j)} \quad v_{i-1}^{(j)} - n_i^{(j)} \quad v_i^{(j)}\right)$$

$$+ \frac{a_{i+1}}{4}\left(n_{i+1}^{(j)} \quad v_{i+1}^{(j)} - n_i^{(j)} \quad v_i^{(j)}\right) + \left(a'_i + a'_{i+1}\right)q_i^{(j)}$$

$$i = 1, 2, \cdots, L \; ; \; j = 1, 2, \cdots, M \; . \qquad (1)$$

$$\frac{d}{dt}\left(k T_i \sum_{j=1}^{M} \delta^{(j)} N_i^{(j)}\right) = \frac{a_i}{4} \sum_{j=1}^{M} k \delta^{(j)} \left(n_{i-1}^{(j)} v_{i-1}^{(j)} T_{i-1} - n_i^{(j)} v_i^{(j)} T_i\right)$$

$$+ \frac{a_{i+1}}{4} \sum_{j=1}^{M} k \delta^{(j)} \left(n_{i+1}^{(j)} v_{i+1}^{(j)} T_{i+1} - n_i^{(j)} v_i^{(j)} T_i\right)$$

$$+ \sum_{j=1}^{M} k \delta^{(j)} T_i \left(a'_i + a'_{i+1}\right) q_i^{(j)}$$

$$i = 1, 2, - - -, L - 1. \qquad (2)$$

where $a_i = c_i A_i$, $a'_i = (1 - c_i) A_i$, k is the Boltzmann constant, δ the number of degrees of freedom of motion of a gas molecule, n_i, v_i and T_i are the number density, the mean thermal velocity and the temperature of the gas molecules in the i th interstice, respectively. The superscript j refers to the purge gas if $j = 1$, or the absorbed gas of kind j otherwise. The number of interstitial spaces is L, and the number of kinds of the absorbed gases is $(M-1)$ so that

$$n_i = \sum_{j=1}^{M} n_i^{(j)} \text{ and } N_i = \sum_{j=1}^{M} N_i^{(j)} \text{ where } N_i^{(j)} = V_i n_i^{(j)} \qquad (3)$$

Finally,

$$q_i^{(j)} = \begin{cases} 0 \ (j = 1) \\ \text{number of outgassing molecules, of kind } j \text{ from the walls binding the } i \text{ th interstice, per unit area and time } (j \neq 1). \end{cases} \qquad (4)$$

Equation (1) states the conservation of mass and Eqs. (2) the conservation of energy.

Since the L th interstice is next to the fuel tank, we may assume that $a_{L+1} = 0$ and $T_L = T_f$, where T_f is the temperature of the fuel tank. Since interstice 1 is the outermost, denoting the number densities, the mean thermal velocities and the temperature of the molecules in the vacuum chamber by $n_c^{(j)}$, $v_c^{(j)}$ and T_c, respectively, we have $n_o^{(j)} = n_c^{(j)}$, $v_o^{(j)} = v_c^{(j)}$ and $T_o = T_c$. Notice that as the volume of the vacuum chamber is very large, $n_c^{(j)}$ $(j \neq 1)$ are increasingly smaller compared to $n_c^{(1)}$ at all times and we may assume that $n_c^{(j)} = 0 (j \neq 1)$. By making this assumption, $v_o^{(j)}$ $(j \neq 1)$ becomes meaningless and it drops out from Eqs. (1) and (2) automatically. Therefore, in Eqs. (1) and (2), we use

$$\begin{cases} a_{L+1} = 0 \ , \ T_L = T_f, \ T_o = T_c, \ v_o^{(1)} = v_c^{(1)} \\ \\ n_o^{(1)} = n_c^{(1)} \ \text{ and } \ n_o^{(j)} = 0 \ \ (j \neq 1) \ . \end{cases} \tag{5}$$

Following $p_i = n_i \, k \, T_i$, where p_i is the pressure in the ith interstice, we may assume that

$$p_i^{(j)} = n_i^{(j)} \ k \ T_i \ \text{ so that } \ p_i = \sum_{j=1}^{M} p_i^{(j)} \tag{6}$$

which is plaussible when the pressure is not too high.

Using Eqs. (3) and (6), if the outgassing rates are expressed in the customary units of pressure times volume per unit area and time denoted by

$$Q_i^{(j)} = k \, T_i \ q_i^{(j)} \tag{7}$$

then, Eqs. (1), (2), and (5) can be written as

$$V_i\left(\frac{1}{T_i}\frac{dp_i^{(j)}}{dt}-\frac{p_i^{(j)}}{T_i^2}\frac{dT_i}{dt}\right)=\frac{a_i}{4}\left(\frac{p_{i-1}^{(j)}}{T_{i-1}}v_{i-1}^{(j)}-\frac{p_i^{(j)}}{T_i}v_i^{(j)}\right)$$

$$+\frac{a_{i+1}}{4}\left(\frac{p_{i+1}^{(j)}}{T_{i+1}}v_{i+1}^{(j)}-\frac{p_i^{(j)}}{T_i}v_i^{(j)}\right)$$

$$+\left(a'_i+a'_{i+1}\right)\frac{Q_i^{(j)}}{T_i}$$

$$i=1,2,\cdots,L\ ;\quad j=1,2,\cdots,M\ . \tag{8}$$

$$V_i\sum_{j=1}^{M}\delta^{(j)}\frac{dp_i^{(j)}}{dt}=\frac{a_i}{4}\sum_{j=1}^{M}\delta^{(j)}\left(p_{i-1}^{(j)}v_{i-1}^{(j)}-p_i^{(j)}v_i^{(j)}\right)$$

$$+\frac{a_{i+1}}{4}\sum_{j=1}^{M}\delta^{(j)}\left(p_{i+1}^{(j)}v_{i+1}^{(j)}-p_i^{(j)}v_i^{(j)}\right)$$

$$+\sum_{j=1}^{M}\delta^{(j)}\left(a'_i+a'_{i+1}\right)Q_i^{(j)}$$

$$i=1,2,\cdots,L-1. \tag{9}$$

$$\begin{cases} a_{L+1}=0,\ T_L=T_f,\ T_0=T_c,\ v_0^{(1)}=v_c^{(1)} \\ p_0^{(1)}=p_c^{(1)}\ \text{and}\ p_0^{(j)}=0\ (j\neq 1)\ . \end{cases} \tag{10}$$

where $p_c^{(1)}$ is the chamber pressure due to the purge gas.

The mean thermal velocities are given by

$$v_i^{(j)} = \left(\frac{8 k T_i}{\pi m^{(j)}}\right)^{1/2}, \quad i = 0, 1, - - -, L; \; j = 1, 2, - - -, M. \qquad (11)$$

where $m^{(j)}$ is the mass of a molecule of the j th kind.

To obtain a solution to the problem, the outgassing rates $Q_i^{(j)}$ must be known a priori, usually determined experimentally.[1,4-7] Outgassing is a process in which gas molecules originally adsorbed or absorbed in a solid material leave that material under reduced pressure or elevated temperature. The outgassing rate of the insulation layers depends on the material and preconditioning of the layers, the temperature, the pressure, the time and the kinds of absorbed gases.*** For a specific material and preconditioning and a specific absorbed gas, $Q_i^{(j)}(T,p,t)$. Around the room temperature range, there is not outgassing at atmospheric or higher pressures. Outgassing occurs when the background pressure is reduced considerably below the atmospheric pressure. The outgassing rate increases as the pressure decreases and attains appreciable values only at very low pressures. However, in very low pressure ranges, the outgassing rate is a weak function of pressure. Therefore, its dependence on the pressure may be approximated by

$$Q_i^{(j)} = \left(1 - \frac{p_i}{p_a}\right) R^{(j)}(T, t) \qquad (12)$$

where $p_i = \sum_{j=1}^{M} p_i^{(j)}$, p_a is the atmospheric pressure and $R^{(j)}$ is the outgassing rates at extremely low pressures.

*** The absorbed gases are mainly water vapor, with small amounts of CO_2 and N_2 (Ref. 7).

The initial conditions associated with the system of Equations (8) and (9) are prescribed according to a specific situation encountered. Usually the evacuation process starts with atmospheric pressure inside the insulation system. In this case, the initial conditions can be written as

$$p_i^{(1)}(o) = p_a\,,\quad p_i^{(j)}(o) = 0\ (j \neq 1),\ i = 1, 2, - - - L$$

$$T_i(0) = T(i)\,,\qquad i = 1, 2, - - -, L - 1. \tag{13}$$

Now, with the $(M + 1)L - 1$ initial conditions given by Eqs. (13) or prescribed otherwise, and with the outgassing rates $\sigma_i^{(j)}$ known, and by using Eqs. (10) and (11), then Eqs. (8) and (9) constitute an appropriate set of $(M+1)L-1$ simultaneous first order differential equations for the same number of unknown functions of time, namely, $T_i(t)\ k=1,2,--L-1$ and $p_i^{(j)}(t),\ i=1,--,L;\ j=1,--,M$.

In some engineering applications, e.g., the Apollo Telescope Mount insulation, the temperature is quite uniform across the entire insulation system, and the gas flow inside the system is nearly isothermal. In this case, the problem reduces to the solution of Eqs. (8) with Eqs. (10) and (11), and the initial conditions (13), when all temperatures are set equal to a constant.

3. Numerical Analysis

In a multilayer insulation system, the number L usually is of the order of 10^2. Thus, the governing Eqs. (8) and (9) consist of a large number of first order differential equations which are non-linear and coupled. The analytical solution of this system of equations can hardly be obtained; therefore, one uses a direct numerical method for its solution.

For simplicity in numerical experiments, we took an isothermal case, and assumed water vapor was the only absorbed gas present ($M = 2$). Furthermore, a hypothetical $R^{(2)}(T_o, t)$ and chamber conditions were used. When the temperature is constant, the energy equations (Eqs. (9)) are not needed, and the problem reduces to the solution of Eqs. (8) with initial conditions (13). In the process of numerical computation, however, the problem of instability occurred. A numerical program using a modified Runge-Kutta method [8] has been set up for this initial value problem. Computer experiments on this scheme showed that the system was stable when the values of $\tau_i^{(j)} = (4 V_i / a_i)(\pi m^{(j)} / 8 k T_o)^{1/2}$, which have a dimension of the time, were large. However, in order to establish numerical stability for small values of $\tau_i^{(j)}$, the step sizes of integration had to be so small that a solution could not be obtained with a reasonable length of computer time. Since in ordinary applications the values of $\tau_i^{(j)}$ are very small, we need to seek some alternative or approximation to the system of Eqs. (8), (9) and (13).

For the case $j = 1$, Eqs. (8) can be written as

$$\frac{dp_i^{(1)}}{dt} - \frac{p_i^{(1)}}{T_i}\frac{dT_i}{dt} = r_{i-1}\frac{p_{i-1}^{(1)}}{\tau_{i-1}} - \frac{p_i^{(1)}}{\tau_i} + r_{i+1}\frac{p_{i+1}^{(i)}}{\tau_{i+1}} - \frac{p_i^{(1)}}{\tau_{ip}} \tag{14}$$

where $\tau_i = \tau(a_i, T_i) = (4 V_i / a_i)(\pi m^{(1)} / 8 k T_i)^{1/2}$, $\tau_{i-1} = \tau(a_i, T_{i-1})$, $\tau_{i+1} = \tau(a_{i+1}, T_{i+1})$ and $\tau_{ip} = \tau(a_{i+1}, T_i)$ have a dimension of the time, and where $r_{i-1} = T_i / T_{i-1}$ and $r_{i+1} = T_i / T_{i+1}$ are dimensionless quantities or order 1.

Let the largest of all the four τ's defined above be τ_m. Define the non-dimensional temperatures and pressures as $T'_i = T_i / T_r$, where T_r is a reference temperature (say the room temperature), and $p'_i = p_i^{(1)} / p_a$. Let τ_e be the time period over which T'_i and p'_i change appreciably, and define the non-dimensional time as $t' = t/\tau_e$ so that dT'_i/dt' and dp'_i/dt' have magnitudes of order 1.

In terms of T'_i, p'_i and t', Eqs. (14) can be written as

$$\frac{\tau_m}{\tau_e}\left[T'_i \frac{dp'_i}{dt'} - p'_i \frac{dT'_i}{dt'}\right] =$$

$$T'_i \left[r_{i-1}\, s_{i-1}\, p'_{i-1} - (s_i + s_{ip})\, p'_i + r_{i+1}\, s_{i+1}\, p'_{i+1}\right] \quad (15)$$

where $s_i = \tau_m / \tau_i$ etc., are dimensionless quantities of order 1.

We see that τ_m is a measure of the relaxation time. If $\tau_m << \tau_e$, the two terms on the left hand side of Eqs. (15) are vanishingly small compared to any term on the right hand side, since the magnitudes of the two terms inside the bracket on the left hand side are of order 1. In this case, component 1 of the gas mixture in the i th interstice is "quasi-steady", which means that at any instant component 1 in interstice i can be considered instantaneously steady and the derivative terms in its governing equation can be dropped. This argument applies to all other components of the mixture in every interstice, i.e., it applies equally well to each equation of Eqs. (8) for cases $j \neq 1$ and Eqs. (9) individually.

As a final step towards completion of this argument, let $1 \leq m \leq L$ and $1 \leq n \leq M$ be two integers such that $\tau_m^{(n)}$ is the largest of all $\tau_i^{(j)}$ defined by

$$\tau_i^{(j)} = (4 V_i / a_i)\,(\pi m^{(j)} / 8 k T_i)^{1/2} \quad (16)$$

Then, the relaxation time of the gas mixture in the entire insulation system τ_s is bounded by $L\,\tau_m^{(n)}$, i.e.,

$$\tau_s \leq L\,\tau_m^{(n)} \tag{17}$$

Denoting the time period over which the properties of the gas mixture change appreciably by τ_t, we can drop all the derivative terms in Eqs. (8) and (9) simultaneously if

$$\tau_s \text{ or } L\,\tau_m^{(n)} \ll \tau_t \quad . \tag{18}$$

Thus, this system of differential equations reduces to a set of algebraic equations.

Now, for ordinary engineering applications, τ_s is of the order $10^{-2} \sim 10^{-1}$ sec., while τ_t is measured by hours. Therefore, condition (18) is usually fulfilled, and Eqs. (8) and (9) reduce to

$$4\left(a'_i + a'_{i+1}\right)\frac{Q_i^{(j)}}{T_i} + a_i\left(\frac{p_{i-1}^{(j)}}{T_{i-1}}\,v_{i-1}^{(j)} - \frac{p_i^{(j)}}{T_i}\,v_i^{(j)}\right)$$

$$+ a_{i+1}\left(\frac{p_{i+1}^{(j)}}{T_{i+1}}\,v_{i+1}^{(j)} - \frac{p_i^{(j)}}{T_i}\,v_i^{(j)}\right) = 0$$

$$i = 1, 2, \cdots, L;\ j = 1, 2, \cdots, M. \tag{19}$$

$$\sum_{j=1}^{M} 4\,\delta^{(j)}\left(a'_i + a'_{i+1}\right)Q_i^{(j)} + a_i \sum_{j=1}^{M} \delta^{(j)}\left(p_{i-1}^{(j)}\,v_{i-1}^{(j)} - p_i^{(j)}\,v_i^{(j)}\right)$$

$$+ a_{i+1} \sum_{j=1}^{M} \delta^{(j)}\left(p_{i+1}^{(j)}\,v_{i+1}^{(j)} - p_i^{(j)}\,v_i^{(j)}\right) = 0$$

$$i = 1, 2, \cdots, L-1. \tag{20}$$

As Eqs. (19) and (20) are algebraic equations, there is no need for the prescription of initial conditions.

To obtain the solution for a particular problem, we first choose a sequence of the time $(t_1, t_2, - - -, t_n)$. The solution at any chosen time, say t_1, is obtained by solving Eqs. (19) and (20) with the chamber conditions and fuel tank temperature at t_1 (see Eqs. (10)) and $R^{(j)}(T, t_1)$ (see Eq. (12)) which are pertinent to that problem. After we finish with the time sequence, we have the pressures and temperatures in all the interstices of the insulation system as functions of the time. If the process is isothermal, one only has to solve Eqs. (19) with the relevant chamber conditions and outgassing rates.

4. Numerical Results and Comparison with Experimental Data

For the purpose of comparison with experiment, we choose examples, the experimental data of which are available.

A circular disk of 1" thick and 6" in diameter is composed of a variety of numbers of insulation sheets of crinkled single-aluminized mylar. The edge of the disk is sealed with a solid insulation sheet (i.e., without perforation). The last layer (the back sheet) is also solid, but the rest of the insulation layers are perforated with a perforation coefficient equal to 0.0138. The perforation holes are 0.09375" in diameter. The distance between two adjacent holes is 0.707" center to center.

The disk is placed in a large vacuum chamber. The chamber and hence the multilayer system (i.e., the disk) are maintained at room temperature all the time, so it is an isothermal process. At the beginning of the experiment, the vacuum chamber and the multilayer system are filled with nitrogen (purge gas), and the pressure inside each interstitial space between two successive insulation layers and the pressure in the chamber are atmospheric. The chamber is then evacuated. The pressure in the chamber and the pressure in the last interstice of the insulation system are recorded as time proceeds.

The outgassing rates, $R^{(j)}$ as functions of the time, of the insulation sheets were obtained before hand by separate experiments. The outgas components are mainly water vapor, with small amounts of nitrogen and carbon dioxide. For simplicity, we assume only one kind of outgas (water vapor) present, i.e., only $R^{(2)}$ has non-zero values. The outgassing rate $R^{(2)}(t)$ of crinkled single-aluminized mylar is shown in Fig. 1.

In our analysis, we use a set of $R^{(2)}(t)$ values at different times successively. To obtain the solution at any chosen time, say t_1, we use the values of $R^{(2)}(t_1)$ and the chamber pressure $p_c^{(1)}(t_1)$ in Eqs.(19). Thus an appropriately chosen set of $R^{(2)}(t)$ and $p_c^{(1)}(t)$ will result in a solution of the $P_i(t)$, the pressure history of the gas mixture inside the multilayer insulation system. However, the $R^2(t)$ values are available only up to $t = 48$ hours; thus, our computations have to stop there.

Theoretical computation includes the pressures $P_i(t)$ inside each interstice, while only the pressure in the last interstice $P_L(t)$, i.e., the backside pressure, is experimentally measured. Therefore, only the comparison for $P_L(t)$ can be made. Comparisons of the theoretical $P_L(t)$ and the experimental data are presented in Figures 2 through 6.

5. Conclusions

First of all, it should be noted that the comparison between the computed and measured values of the p_L's presented in Figs. 2 through 6 cannot be taken seriously, since it is known that the experiment for the determination of the outgassing rate was not appropriately performed; thus, the values of $R^{(2)}(t)$ presented in Fig. 1, upon which our calculation was based, are not reliable.‡ Nevertheless, Figs. 2 through 6 serve to show a qualitative comparison and to indicate some possible experimental errors.

It can be seen from the figures that at early times the computed p_L is much higher than the experimental values. However, the computed and the measured values are coming closer and closer together as time proceeds, and good agreement is established after a reasonably long time. Since the effect of preconditioning on the outgassing rate is likely to be a weak function of time when t is large, one probable and important course of experimental discrepancy would arise from different preconditionings of samples, i.e., the samples for the measurement of p_L (t) and the sample for the determination of $R^{(2)}(t)$ were differently pre-treated. Another source of error would be the contamination of equipments inside the vacuum chamber.

It is believed that agreement between the theory and experiment can be achieved if, with special attention to preconditioning, a set of consistent experiments is performed.

---

‡At the time of the writing of this report, the Marshall Space Flight Center is planning to reconduct the outgassing rate experiment.

References

1. Lindquist, C. R., "Superinsulation Systems for Cryogenic Test Tank," NASA Contract NAS8-11740, June 1964 - January 1966.
2. Coston, R. M., "A Study on High-Performance Insulation Thermal Design Criteria," NASA Contract NAS8-20358, Vol. 1, Lockheed Missiles and Space Company, Sunnyvale, California, June 1967.
3. Hyde, E. H., "Multilayer Insulation Thermal Protection Systems Technology," NASA TMX-64561, Vol. 4, Report No. 2, 1972.
4. Brogan, J. J., "Investigation Regarding Development of a High Performance Insulation System," NASA Contract NAS8-20758, Third Quarterly Report, Lockheed Missiles and Space Company, Sunnyvale, California, Nov. 1967-Feb. 1968.
5. Santeler, D. J., "Outgassing Characteristics of Various Materials," Transactions of Fifth National Symposium on Vacuum Technology, Pergamon Press, New York, 1958, pp. 1-8.
6. Dayton, B. B., "Relations Between Size of Vacuum Chamber, Outgassing Rate and Required Pumping Speed," Transactions of the Sixth National Symposium on Vacuum Technology, Pergamon Press, New York, 1959, pp. 101-119.
7. Glassford, A. P. M., "Outgassing Behavior of Multilayer Insulation Materials," J. Spacecraft and Rockets, Vol. 7, No. 12, Dec. 1970, pp. 1464-1468.
8. Gill, S., Proc. Cambridge Philos. Soc., Vol. 47, 1951, pp. 96-108.

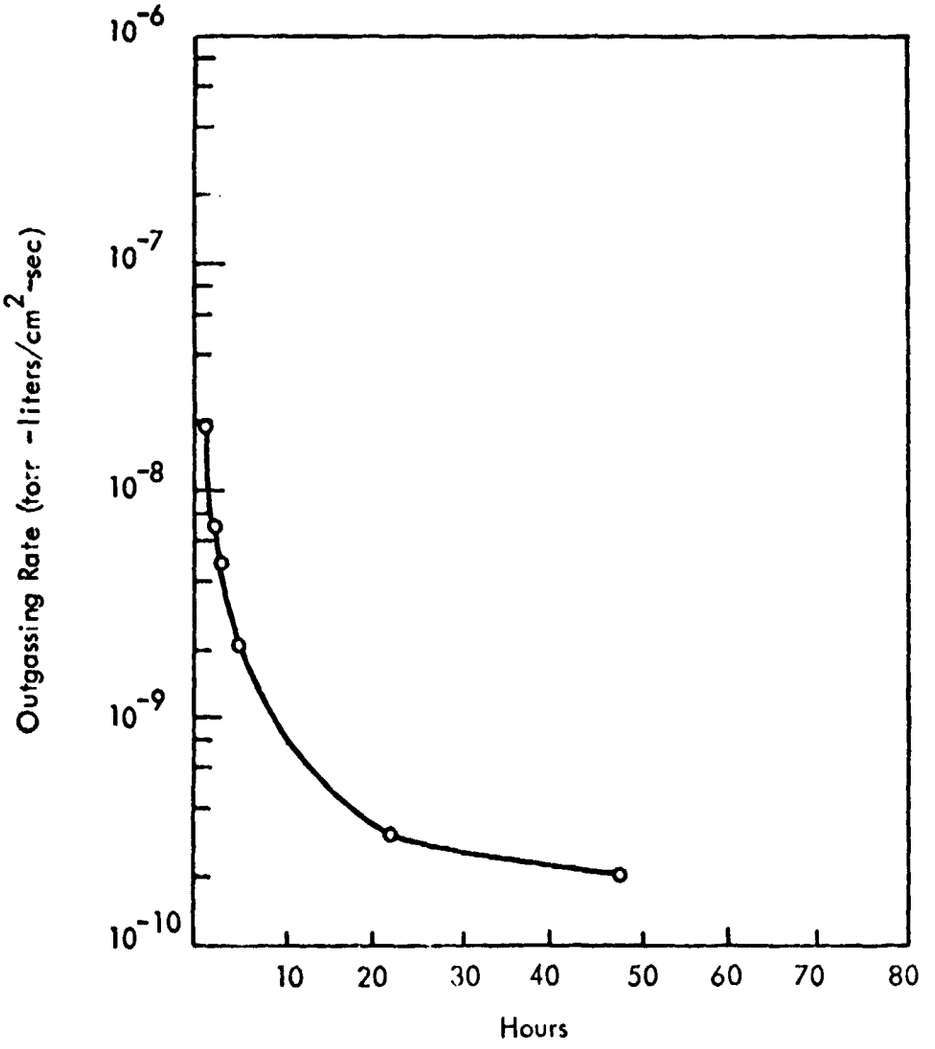

FIG. 1. Outgassing Rate for Crinkled Single-Aluminized Mylar.

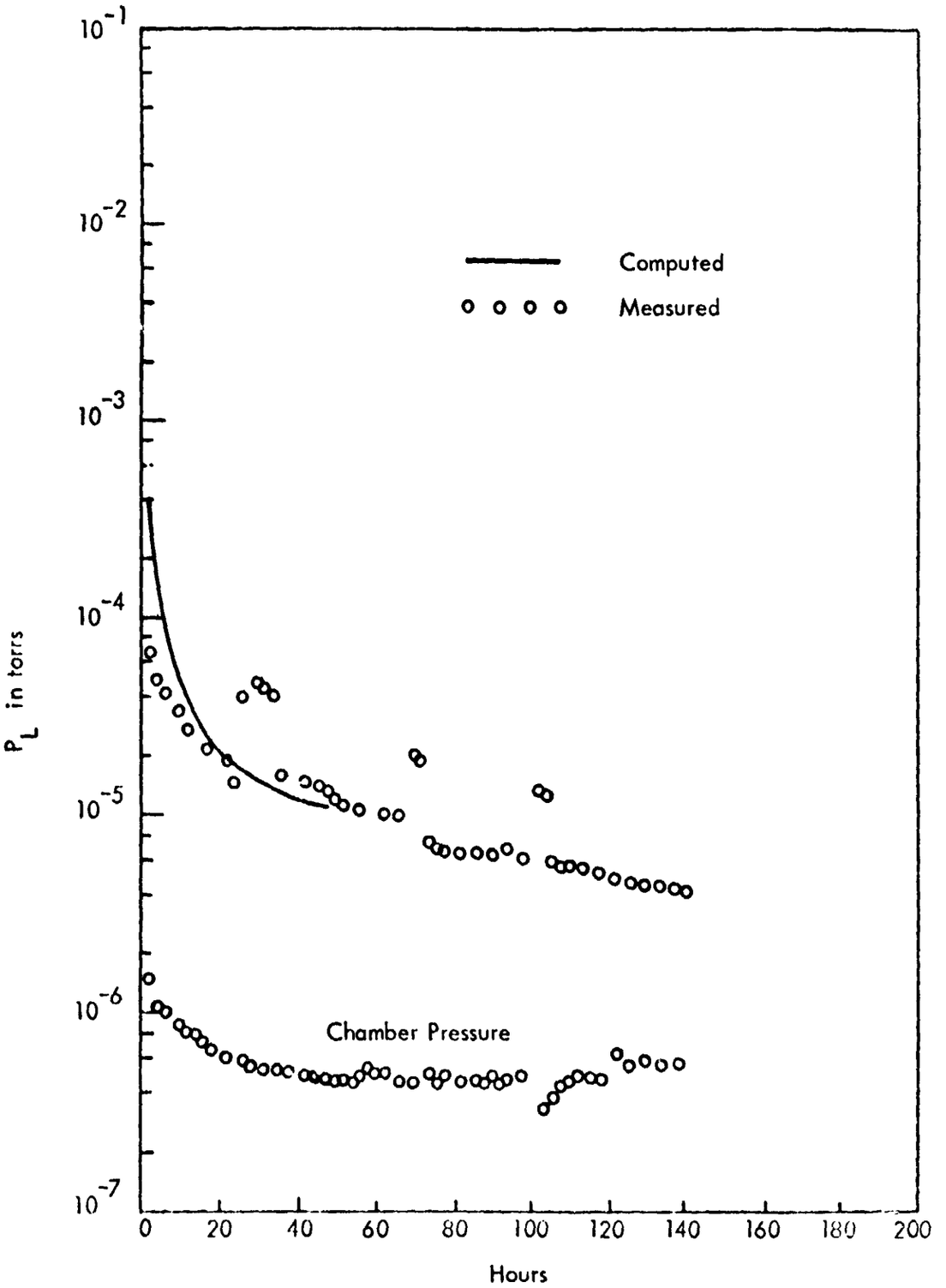

FIG. 2. Comparison of Computed and Measured Backside Pressures, 10-Layer Sample.

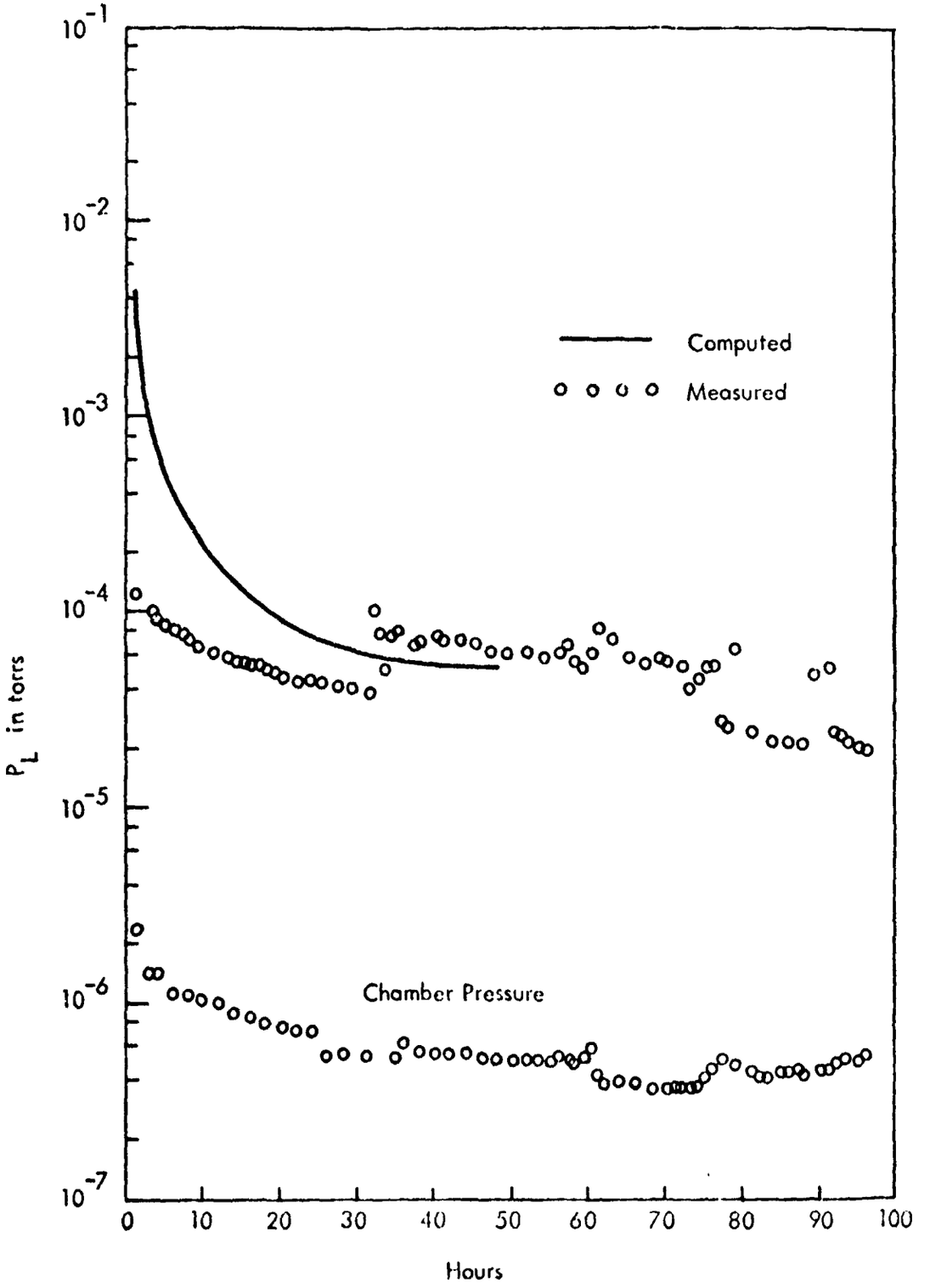

FIG. 3. Comparison of Computed and Measured Backside Pressures, 20-Layer Sample.

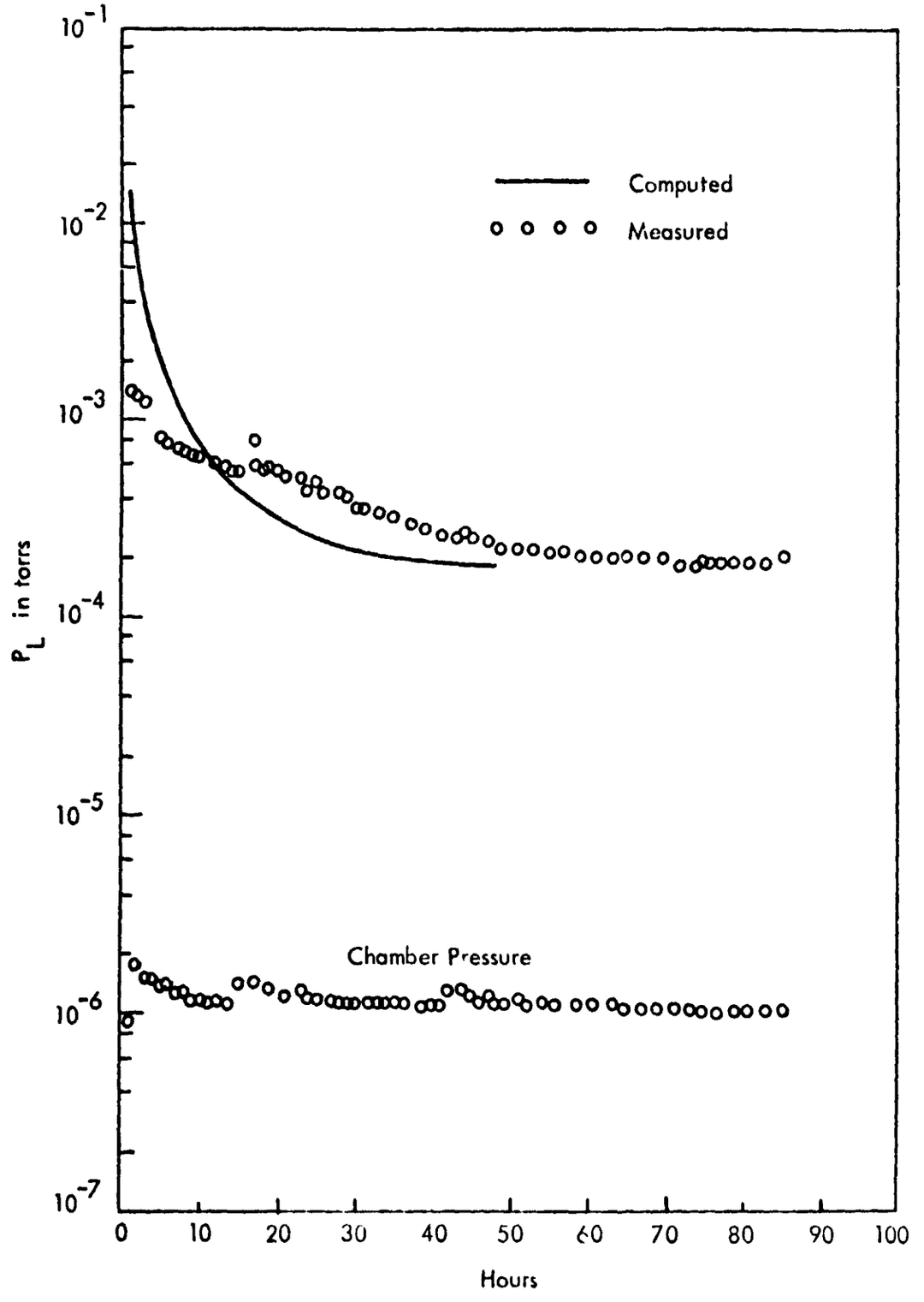

FIG. 4. Comparison of Computed and Measured Backside Pressures, 35-Layer Sample.

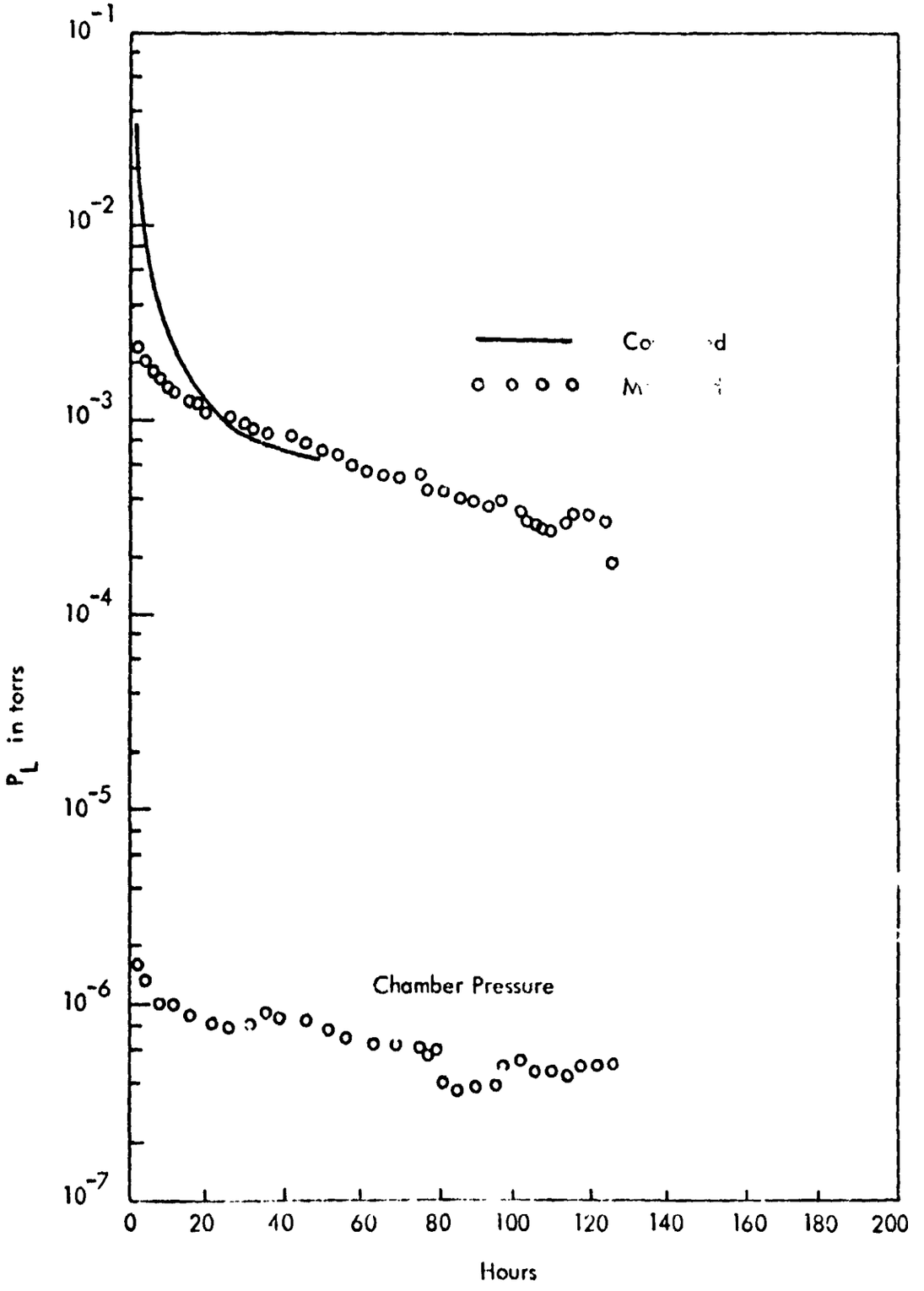

FIG. 5. Comparison of Computed and Measured Backside Pressures, 70-Layer Sample.

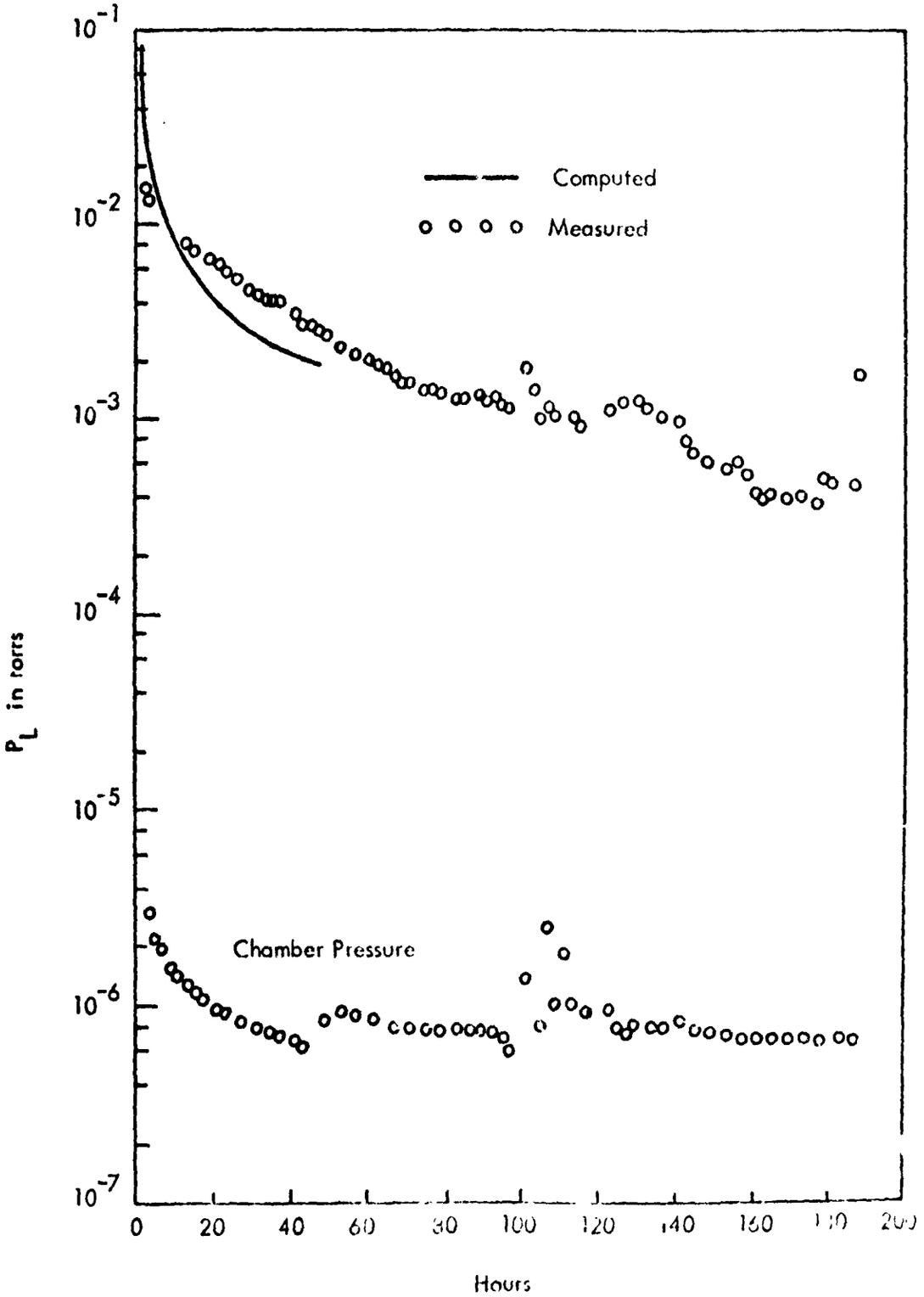

FIG. 6. Comparison of Computed and Measured Backside Pressures, 105-Layer Sample.

UAH-MSFC/NASA Cooperative Agreement

Modification No. 1

Project II

Study of Deposition Model of Frost and Ice From Humid Gas in Ducts

Final Report

by

Bhuminder Singh

and

C. C. Shih

Department of Fluid & Thermal Engineering
School of Graduate Studies and Research
The University of Alabama in Huntsville
P. O. Box 1247
Huntsville, Alabama 35807

INTRODUCTION

Heat exchangers are an essential part of the process of cooling various components in space vehicles. Since, in any design related to space travel, ways of reducing weight and volume are always of utmost importance, a concept that would lead to light and compact heat exchangers should certainly be looked into. One possibility that has been suggested is the use of cryogenic liquids as the coolant in these heat exchangers. This offers an excellent possibility for improved performance and reduction in weight and volume since cryogenics provide extremely low temperatures. This concept appears even more attractive when one considers the fact that cryogenics are already used as fuel in space vehicles and hence readily available to serve a dual purpose. However, when humid air comes in contact with a cryogenically cooled surface, frost forms rapidly on the surface and may eventually plug up the system and render it useless until the frost is removed. Therefore, the design of such a heat exchanger would require detailed information regarding this frost formation. This is where the purpose of this study comes in.

Objectives:

The basic objective is to study the frost formation on super-cooled surfaces as a function of time, air velocity, air inlet and outlet temperatures. This would be done analytically as well as experimentally to arrive at empirical relations that would predict heat transfer coefficients and rate of frost growth for different conditions.

Experimental Set-Up:

The study began with a crude experimental model (Figure 1) to gain a perspective of the problem. The set-up primarily consisted of a blower providing air flow for the heat exchanger. The heat exchanger consisted of two flat plates and these plates were cooled by the use of dry ice in an

acetone bath. However, certain problems were realized immediately. First, the room air did not supply sufficient moisture to show a significant frost build up. Tests were conducted with Scott Phase Heat Exchanger (Model 9058) to investigate its use as a source of moisture for the system. This equipment proved to be successful in providing sufficient moisture to enable us to observe for the first time an actual plug-up of the air passage due to frost build-up. Photographs of this passage were taken at different intervals. This plug-up was observed for various width spacing of the two plates. In order to see how thick the frost would get before it begins to act as an insulator, it would have been necessary to have a very large width between the plates and then maintain the humid flow and low temperatures for several hours. This was not possible for the existing set-up due to the problem of boil-off of the coolant and hence the inability to maintain cold plates for the required duration of time.

Another problem that was realized was the fact that this set-up had no means of recording the frost growth. Thought was given to various methods of recording this frost growth. One such method consisted of measuring capacitance change between the plates and relating it to frost build-up. Hewlett Packard Universal Bridge Instruments (Model 4260A) was utilized for recording such capacitance changes. However, it was soon discovered that the capacitance between the plates changed not only due to frost build-up, but was also affected by the plexiglass casing, as well as any changes in the flow rate or temperature of the air passing between the plates. It was therefore decided that this method was not feasible.

Having realized that this set-up had no means of recording frost growth the air velocity, humidity and temperature, and that the existing test section allowed too much coolant boil-off and had no provisions for draining the water from the melting of frost at the end of an experiment, it was

decided to design and assemble a new system and a new test section. A considerable amount of time was spent towards designing such a system, and the final arrangement is shown in Figure 2.

Compressed air is used as the source of flow for the system. This eliminates the need for a blower. A pressure regulator and a gate valve are used to control the flow rate. This flow rate is measured using a Cox Turbine meter and a frequency counter. Pressure and temperature are recorded at this point to convert from ACFM to SCFM. This air supply is now passed through an 8" x 10" rectangular duct where it is heated to a desired temperature by a variable 5 kw duct heater (H.W. Tuttle Co.). Relative humidity is controlled by using a power spray humidifier and recorded on a Serdex Hygrothermograph, before being sent to the test section. A picture of the assembled system is shown in Figure 3.

The new test section has been designed but not yet constructed. A picture of the proposed test section is shown in Figure 4. When assembled, this test section will have the same two flat plates forming a rectangular passage. However, the new concept has an air passage below and above the test passage to circulate warm air eliminating fog formation and making it possible to record visually, from above, the frost growth at various locations along the test section. Liquid Nitrogen will be used instead of dry ice to provide the cryogenic temperatures. (The boxes contain the spray-on foam insulation (SOFI) to reduce boil-off.) This new test section has an easy arrangement for changing the spacing of the two plates without disassembling the whole thing. The handles that hold the plates in place travel in grooves and simply need to be moved in or out to change the width of the gap.

Analytical Study:

The analysis of an approximate model for the growth of a deposited layer on the cryogenic surface has been initiated, the details of which have been

previously reported in an interim report (Mod. I, Project II, October 1972).

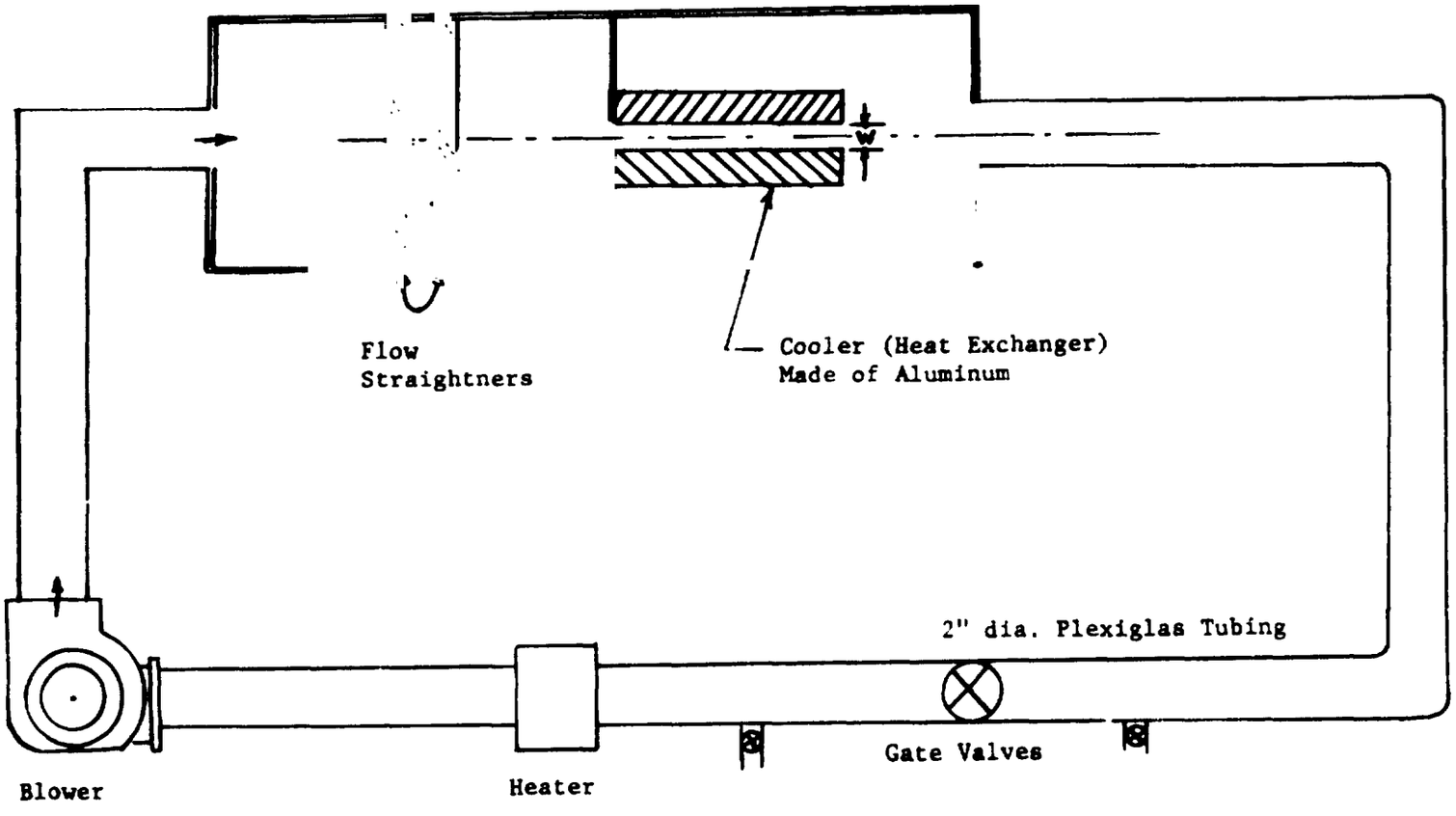

FIGURE 1. CRUDE EXPERIMENTAL MODEL OF HEAT EXCHANGER STUDY

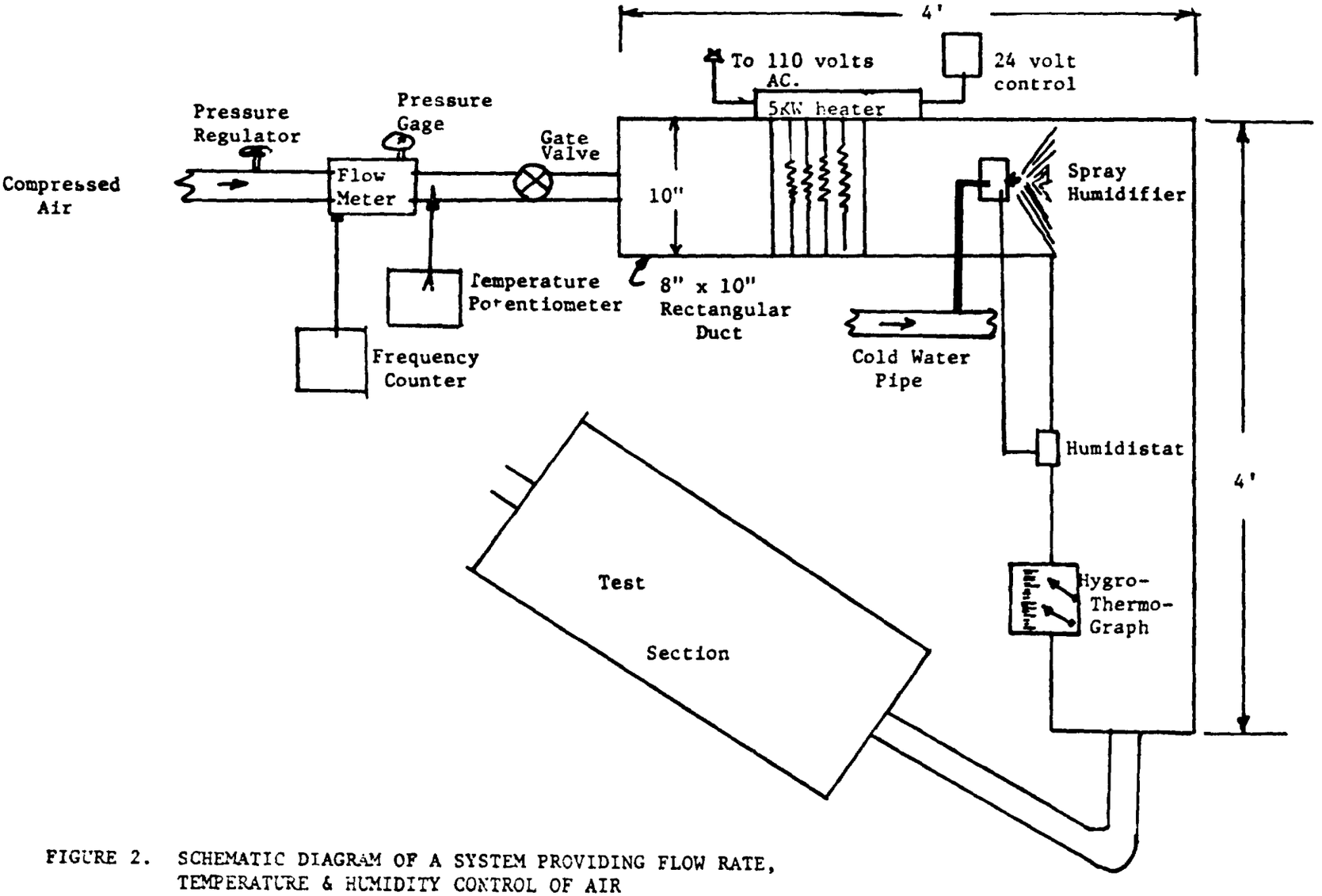

FIGURE 2. SCHEMATIC DIAGRAM OF A SYSTEM PROVIDING FLOW RATE, TEMPERATURE & HUMIDITY CONTROL OF AIR

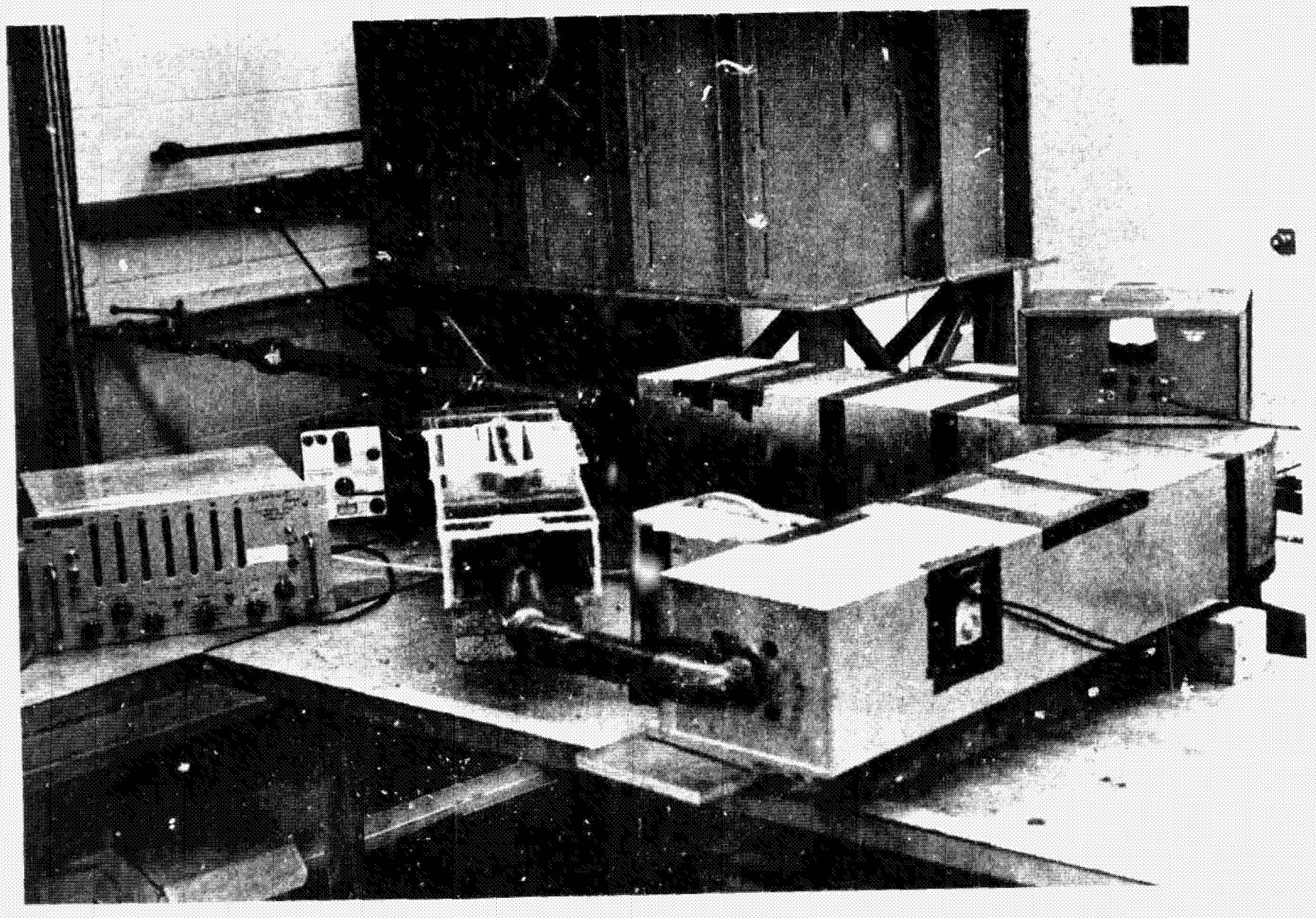

FIGURE 3. PHOTOGRAPH OF THE AIR CONTROL SYSTEM

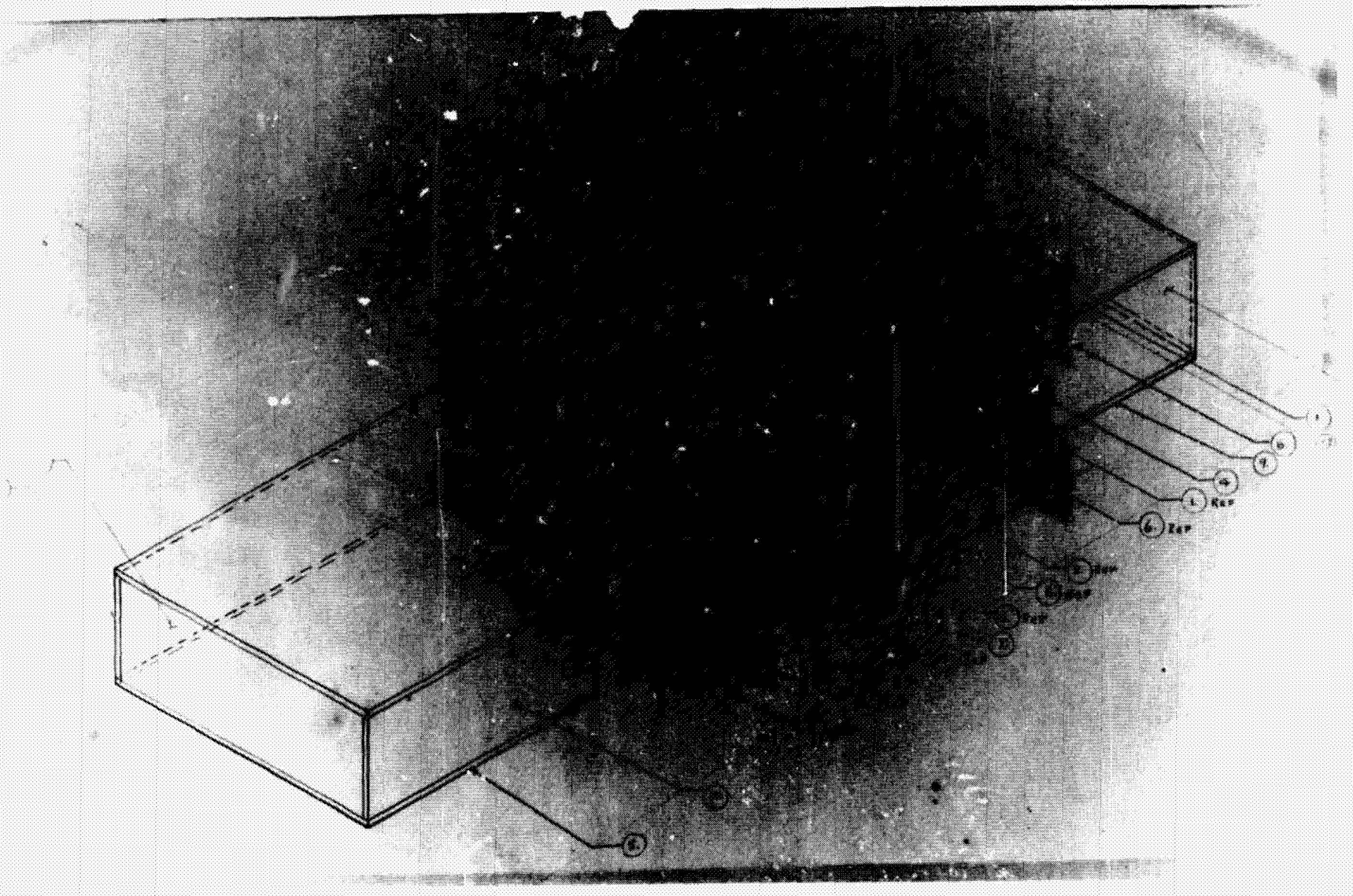

FIGURE 4. PROPOSED TEST SECTION

UAH-MSFC/NASA Cooperative Agreement

Modification No. 1

Project III

Analysis of Thermal Environment in the Thrustor Cavity of Space Vehicles

Final Report

by

J. N. Chiou

and

J. J. Brainerd

Department of Fluid & Thermal Engineering
School of Graduate Studies and Research
The University of Alabama in Huntsville
P. O. Box 1247
Huntsville, Alabama 35807

FOREWORD

The work described in this report is part of a continuing effor being carried out at UAH. The participants in this study have maintained a close liaison with Mr. Bob Fisher and Mr. Jerry Vanneman of NASA-MSFC, . The purpose of this close liaison has been to discuss problems, results, and new techniques in order that the results of this study be as beneficial to this group as possible. Consequently, many informal recommendations have been made, which may or may not be formalized in this report.

TABLE OF CONTENTS

Chapter		Page
	FOREWORD	i
I.	INTRODUCTION	1
	1.1 The Problem	1
	1.2 Literature Survey	1
	1.3 Experimental Program	2
II.	ANALYSIS	3
	2.1 Fundamental Features of the Flow	3
	2.2 Horseshoe Vortex Model	4
	2.3 Vortex Strength	7
	2.4 Experimental Results	9
	2.5 Cavity Shape	11
III.	APPLICATION OF 2-D THEORY	12
	3.1 Modified 2-D Theory	12
	3.2 Zero Incidence Cases	15
	3.3 Angle of Attack Cases	16
IV.	RESULTS	18

NOMENCLATURE

a	Cavity width
b	Cavity depth
D_j	Cavity opening diameter in axially-symmetric nozzle
$\overline{F^2}$	Root-mean square of the surface velocity over the perimeter of the cavity
L	Reattachment zone length (equ. 12)
Me	Mach number of the external flow
Re	Reynold's number
Re_L	$U_d L/\nu_c$
Sty	Local Stanton number $g/[\rho_c v c_p (T_d-T_w)]$
Taw	Adiabatic wall temperature
To	Stagnation temperature of flow
Tw	Cavity wall temperature
v	Local velocity outside boundary layer on cavity wall
X_o	Effective running length
γ	Ratio of specific heat (c_p/c_v)
Γ	Circulation
ω	Vorticity
θ	Angle counting counterclockwise from axis of symmetry

Subscripts

c	Condition in cavity
d	Condition for dividing streamline
e	Condition for external flow

m	Modified theory value
∞	Condition for free stream

INTRODUCTION

1.1 The Problem

The problem to be studied stems from the requirement for the control system thrustors of a space shuttle type vehicle, necessary for exo-atmospheric flight control, to be buried within the heat shield of the vehicle so that interference heating will be reduced during flight in the atmosphere. The geometry of a typical installation is illustrated in Figure 1. During atmospheric flight, the non-firing thrustor nozzle is simply a cavity in the surface of the vehicle. The interaction of the hypersonic external flow with the cavity produces excess local heating which must be ameliorated.

Mechanical systems, such as a cover that slides over the nozzle exit, and active cooling systems introduce other problems besides adding undesirable weight and complexity to the vehicle. The simple expedient of increasing heat shield thickness in the region of the cavity would ultimately imply additional ablation in the area and a probable change in nozzle size or shape from flight to flight. This may require additional refurbishment before each flight.

This study, therefore, is aimed at determining the mechanisms involved in producing the high local heating rates in and around the thurstor nozzle in non-firing condition. In such a case, the nozzle is treated simply as a cavity.

1.2 Literature Survey

A survey of the literature on this and related problems has revealed that very few results applicable to this particular problem are available. Of the papers reviewed, only those referenced in this report appear to have direct consequence for this study.

1.3 Experimental Program

A test program, conducted at AEDC by personnel of General Dynamics, Corp., has produced some results directly applicable to this study. In order to provide a basis for comparison or for development of empirical relations, a short study was made to compare the flow conditions in the wind-tunnel studies with flight conditions. Of particular concern was the question of whether the boundary layer ahead of the cavity was laminar or turbulent in either the wind tunnel or flight regimes. A map of these conditions is shown in Figures 2 and 3. The wind tunnel conditions are for the von Karman Facility, Tunnel B, at AEDC[1]. The flight conditions are for a typical reentry corridor,[2] with no special attempt to relate the reentry trajectory to the space shuttle vehicle.

In the wind tunnel tests and in the flight regime, it is to be expected that the boundary layer ahead of the nozzle cavity will be fully developed and turbulent. In flight, but not in the wind tunnel, the boundary layer probably would contain significant amounts of ablation products. No attempt is made to account for the influence of ablation or surface heating ahead of the nozzle area, except to account for the total temperature profile through the boundary layer and, hence, the total pressure profile.

Since the analysis of the experimental data is being carried out at General Dynamics, no general discussion of the results will be made here. In so far as possible, comparisons of the results of this study are made with the raw data of the experiments.[3] These confirm the qualitative features of the flow derived from theoretical analysis.

ANALYSIS

2.1 Fundamental Features of the Flow

In the flight vehicle, the thrustor nozzles are to be installed in curved surfaces. Presumably, the local radius of curvature of the body will be sufficiently large cf. the nozzle diameter so that the effects of surface curvature will be at most of secondary importance in this problem. The wind tunnel test program centered mainly on axially-symmetric nozzles set into a flat-plate model. In this study, only one basic configuration is considered. This is the axially-symmetric nozzle cavity set into a flat plate with the nozzle axis normal to the plate surface, as in Fig. 1. The flow would be two-dimensional in the absence of the cavity. The disturbance produced by the cavity is three-dimensional, which greatly adds to the complexity of the problem.

Sketches of a two-dimensional cavity flow and the central plane of the present problem are shown in Fig. 4. In the two-dimensional problem, the boundary layer separates from the upstream edge of the cavity. The dividing streamline leaves the separation point and intersects the downstream surface of the cavity, at a stagnation point. The location of the stagnation point depends upon several parameters such as cavity height and cavity width. But, in the steady state 2-D solution, the stagnation streamline is the separation streamline. The flow within the cavity circulates about a vortex core, driven by the shearing stress along the dividing streamline.

In the three-dimensional case, fluid may move in the y direction so that a net mass may be injected into the cavity in the central plane. In a steady

state, the mass flowing into the cavity near the center line must flow out of the cavity at some distance from the central plane. The symmetry of the cavity clearly shows that stagnation should occur only in the central plane, so that the lateral flow would be expected to occur. The injected mass flow would increase the angular momentum of the flow in the cavity, thereby strengthening the vortex within the cavity. This vortex must exit the cavity with the outflow and be washed downstream. The resultant vortex shape is reminiscent of the classical horseshoe vortex of a lifting wing of finite span. (Fig. 5) A crude model has been devised to indicate the influence of this vortex on the pressure distribution in the neighborhood of the cavity. The model is discussed in some detail in the next section of this report, including a comparison with experimental results. No attempt has been made to include compressibility effects, or the interaction of the trailing vortex with the boundary layer.

The strength of the vortex within the cavity is difficult to ascertain. Values may be inferred from two-dimensional results, but great care must be exercised in order to avoid erroneous conclusions. A discussion of two-dimensional and axially symmetric (annular cavity) studies is presented in a succeeding section of this report. As a result of these studies, some tentative conclusions may be drawn, particularly in reference to future experimentation.

2.2 Horseshoe Vortex Model

The vortex within the cavity in the three-dimensional case must extend "to infinity," close on itself, or end on a solid wall, according to a theorem

due to Helmholtz. It has also been shown that in viscous flow, a vortex line may end on a solid boundary only at a stagnation point. Consequently, the vortex generated in the cavity in the case under consideration must have the form as described earlier (Fig. 5).

The horseshoe vortex must be one of the dominant features of the cavity-boundary layer interaction. The flow induced by the vortex would modify pressure distributions and velocity fields to a significant degree. Viscosity and compressibility would modify these effects, of course.

A crude initial model was devised by considering the superposition of a uniform flow on the flow due to a horseshoe vortex in steady, potential flow. Viscosity, compressibility and body forces are neglected. The boundary condition that there be no flow through the surface is imposed by the method of images. The cavity was not included in the geometry.

The velocity field induced by a horseshoe vortex lying in an xy plane at a height z_1 above the surface is given by [4]:

$$\vec{V}_1 = \frac{\Gamma}{4\pi}\left[\frac{(z-z_1)\vec{i} + (x-x_1)\vec{k}}{(z-z_1)^2 + (x_1-x)^2}\left\{\frac{y-y_1}{\sqrt{(x-x_1)^2+(y-y_1)^2+(z-z_1)^2}} - \frac{y-y_2}{\sqrt{(x-x_1)^2+(y-y_2)^2+(z-z_1)^2}}\right\}\right.$$

$$+ \frac{(z-z_1)\vec{j} + (y_1-y)\vec{k}}{(z-z_1)^2 + (y_1-y)^2}\left\{1 + \frac{x-x_1}{\sqrt{(x-x_1)^2+(y-y_1)^2+(z-z_1)^2}}\right\}$$

$$\left. - \frac{(z-z_1)\vec{j} + (y_2-y)\vec{k}}{(z-z_1)^2 + (y_2-y)^2}\left\{1 + \frac{x-x_1}{\sqrt{(x-x_1)^2+(y-y_2)^2+(z-z_1)^2}}\right\}\right] \quad (1)$$

where Γ is the circulation. The model is illustrated in Fig. 6. In comparison of this initial model with the actual flow geometry, the length of segment A-B of the horseshoe vortex is taken as being equal to the nozzle exit diameter.

Since the image system utilized above guarantees that there be no flow through the surface z = 0, this model shows no flow into the cavity. In order to obtain a downwash velocity over the cavity opening, an additional line vortex segment is superimposed, on the flow field in the upper half plane. This new vortex segment is parallel to the segment AB, at a distance equal to z, below the cavity surface. Thus the velocity vector is obtained:

$$\vec{V} = U_\infty \vec{i} + \frac{\Gamma}{4\pi}\left[\frac{(z-z_1)\vec{i} + (x_1-x)\vec{k}}{(z-z_1)^2 + (x_1-x)^2}\left\{\frac{y-y_1}{\sqrt{(x-x_1)^2+(y-y_1)^2+(z-z_1)^2}}\right.\right.$$

$$\left.\left. - \frac{y-y_2}{\sqrt{(x-x_1)^2+(y-y_2)^2+(z-z_1)^2}}\right\}\right.$$

$$- \frac{(z+z_1)\vec{i} + (x_1-x)\vec{k}}{(z+z_1)^2 + (x_1-x)^2}\left\{\frac{y-y_1}{\sqrt{(x-x_1)^2+(y-y_1)^2+(z-z_1)^2}} - \frac{y-y_2}{\sqrt{(x-x_1)^2+(y-y_2)^2+(z-z_1)^2}}\right\}$$

$$+ \frac{(z-z_1)\vec{j} + (y_1-y)\vec{k}}{(z-z_1)^2 + (y_1-y)^2}\left\{1 + \frac{x-x_1}{\sqrt{(x-x_1)^2+(y-y_1)^2+(z-z_1)^2}}\right\}$$

$$- \frac{(z+z_1)\vec{j} + (y_1 - y)\vec{k}}{(z+z_1)^2 + (y_1 - y)^2} \left\{ 1 + \frac{x - x_1}{\sqrt{(x - x_1)^2 + (y - y_1)^2 + (z + z_1)^2}} \right\}$$

$$- \frac{(z-z_1)\vec{j} + (y_2 - y)\vec{k}}{(z-z_1)^2 + (y_2 - y)^2} \left\{ 1 + \frac{x - x_1}{\sqrt{(x - x_1)^2 + (y - y_2)^2 + (z - z_1)^2}} \right\}$$

$$+ \frac{(z+z_1)\vec{j} + (y_2 - y)\vec{k}}{(z+z_1)^2 + (y_2 - y)^2} \left\{ 1 + \frac{x - x_1}{\sqrt{(x - x_1)^2 + (y - y_2)^2 + (z + z_1)^2}} \right\} \Bigg] \quad (2)$$

In this model the compressibility, the boundary conditions on the cavity walls, and the boundary layer upstream of the cavity have not been taken into account. The pressure at any point is obtained from the incompressible Bernoulli Equation.

2.3 Vortex Strength

Since the velocity and pressure fields in the vortex model are dependent upon the strength of the vortex, Γ, (circulation) some method for predicting the value of Γ must be specified. In the absence of any theoretical study which would specify Γ for the geometry of this problem, an appeal is made to the qualitative similarity between the flow in the plane of symmetry and the flow in a two-dimensional problem.

Burggraf[5] has given the following relation for the vorticity, ω, in a two-dimensional rectangular cavity:

$$\omega = \frac{U_\infty}{a}\left[\frac{0.0615}{(1+b/a)}\ \frac{(a/X_o)^{2/3}}{\overline{F^2}}\right]^{1/2} \tag{3}$$

where a is the width of the cavity, b is the depth of the cavity, X_o is the "effective running length" to the separation point (in our case, the distance from the leading edge of the plate to the edge of the cavity), and $\overline{F^2}$ is the root-mean-square of the surface velocity over the perimeter of the cavity.

The values of $\overline{F^2}$ given by Burggraf are:

b/a	1/4	1/3	1/2	1	2	3	4
$\overline{F^2}$	.01092	.01732	.03122	.07029	.12488	.15583	.17466

For constant values of U_∞, X_o, and b, the variation of the vorticity ω with cavity width, a, may be obtained from

$$\frac{\omega}{\omega_1} = \left(\frac{a_1}{a}\right)\left[\frac{(1 + b/a_1)\ \overline{F_1^2}}{(1 + b/a)\ \overline{F^2}}\right]^{1/2} \tag{4}$$

where the subscript 1 denotes a reference condition. With a_{ref} taken as being equal to b, this variation of ω with a is shown in Fig. 8.

The heat transfer rate on the reattachment (downstream) wall of the cavity is given by Hodgson[6] as:

$$\frac{q}{q_1} = \left(\frac{a}{a_1}\right)^{3/4} \tag{5}$$

This variation is also shown in Fig. 8.

Burggraf's theory is based upon the plane, inviscid, incompressible, but rotational, flow over a rectangular cavity. According to his theory,

the heat transfer rate depends only on the cavity width-to-depth ratio. Hodgson includes compressibility. His results indicate that the heat transfer rate may vary with cavity width, even with b/a fixed, thus revealing a scaling effect.

A comparison of the heat transfer rates on the reattachment wall predicted by these two-dimensional theories with the rates obtained in the plane of symmetry in the three-dimensional tests in a wind tunnel are shown in Fig. 9. Two items are immediately indicated by this comparison: 1) the test data is much steeper in the reattachment zone than that predicted by either Burggraf's or Hodgson's theory; and 2) the tests show a decrease in reattachment heating with decreasing nozzle diameter as evidenced by tests with a two inch diameter nozzle, and tests with a one inch diameter nozzle. Hence, scaling may be a very important factor in the application of the wind tunnel test results to the flight vehicle.

The vorticity predicted by Burggraf's two-dimensional theory was taken to predict the circulation Γ of the horseshoe vortex in the three-dimensional model discussed earlier. The pressure distribution obtained from this model are shown in Fig. 10. Experimental results, shown in Figs. 11 - 21, show qualitative agreement.

2.4 Experimental Results

Tests of the axially symmetric nozzle cavity in a flat plate at various angles of attack, were conducted in the AEDC-VKF Tunnel B, for various Reynolds Numbers and at a nominal Mach Number of 8. Wind tunnel operating conditions for the various tests are listed in Table I. The flow conditions

on the flat plate for the ten cases shown in this report are listed in Table II. Isobars and isotherms in the vicinity of the cavity for these ten cases are shown in Figs. 11 - 21.

The major qualitative features of the pressure field in these tests are predicted by the horseshoe vortex model of the flow. Of particular interest in this respect is the high pressure zones just outside the cavity at $\theta = 0^{o}$. Where the theory shows a decreasing pressure, the experiment shows a low pressure on the cavity lip and a rising pressure downstream. This discrepancy could be due to separation as the reattached flow tries to negotiate the sharp lip of the cavity exit. In any event, the agreement is remarkable in view of the crudeness of the theoretical model. This clearly demonstrates that the horseshoe vortex is the key feature of the flow field.

One aspect of the test results is very interesting. In an effort to reduce the peak heating rate in the cavity, which occurs at the reattachment point, cold gas was bled (i.e., at low thrustor chamber pressure) through the nozzle in cases 2 and 3. With increasing bleed rate the stagnation point (reattachment point) moved farther into the cavity and the reattachment wall temperature increased. Thus the nozzle bleed aggravated the heating problem instead of ameliorating it. The horseshoe vortex model of the flow explains this phenomenon. Since for the bleed cases (as opposed to thrustor firing) the stagnation pressure of the bleed gas is much, much less than the stagnation pressure of the external flow. As indicated in Fig. 22, the recirculating gas is not much influenced by the bleed gas which

must separate from the downstream (reattachment) wall just above the nozzle throat. Consequently, all of the bleed gas must be directed upward along the upstream wall. This injection of the bleed gas increases the angular momentum of the cavity flow, and therefore increases the vortex strength. The stronger vortex, in turn pulls in more of the external flow, again increasing the angular momentum in the cavity. The new stagnation streamline, moreover, originates higher in the upstream boundary layer so that it has a higher stagnation temperature than the streamlines closer to the wall, due to heat transfer to the plate.

2.5 Cavity Shape

Thomke[7] has studied the flow of turbulent boundary layers flowing over axially-symmetric cavities (annular grooves cut into the surface of a right-circular cone). The experimental tests were conducted at Mach Numbers of 2.0, 2.5, 3.0, and 4.0 and wind tunnel unit Reynold's Numbers of 0.95, 1.02, 1.36, 1.43, and 1.30 million. A comparison of pressure distributions taken at $M = 2.0$, $R_e = 0.95 \times 10^6$ per inch for two cavity shapes is shown in Fig. 23.

The test results clearly show that rounding the reattachment wall produces a much flatter (almost constant) pressure distribution along the cavity floor. Additionally, the rounded corner results in a lower peak pressure, and the point of maximum pressure being moved downstream. These results would imply that rounding the corner would reduce heating in or near the cavity.

APPLICATION OF 2-D THEORY

3.1 Modified 2-D Theory

As indicated before, the flow over the actual thrustor nozzles and over the axially-symmetric nozzles mounted in the wind tunnel models is three-dimensional. But presently, there is no theoretical study on the three dimensional cavity flow which can be used to predict the heat transfer rate to the thrustor nozzle walls. Since, due to symmetry of the cavity, the flow would stagnate in the central plane, the central plane would have the most severe heating caused by the flow. Further, the flow in the plane of symmetry is qualitatively similar to a two-dimensional flow. Hence, an attempt was made to utilize the existing two-dimensional theory coupled with the experimental data, to predict the reattachment heating on the central plane of the thrustor nozzles.

From the literature survey, it was found that Hodgson's[6] theory was the most applicable to this study. The model chosen in Hodgson's theory is shown in Fig. 24. It is similar to that used by Chung and Viegas,[8] who neglected the oncoming boundary layer. The resulting expression for the velocity down the reattachment wall is

$$\frac{v(y)}{u_d} = 1 - 0.189 \exp\left(-5.3 \frac{y}{L}\right) - 10.6 \sum_{n=1}^{\infty} \frac{\exp\left[-y/L \left(9.87 n^2 + 28.1\right)^{1/2}\right]}{9.87 n^2 + 28.1} \qquad (6)$$

The effect of the upstream boundary layer is accounted for through its influence on the dividing streamline velocity U_d, which can be obtained from the analysis of Denison and Baum.[9] A least-square curve fit of Denison and Baum's result has been given by C. D. Engel[10] as

$$\frac{U_d}{U_e} = a_0 + a_1\xi + a_2\xi^2 + a_3\xi^3 + a_4\xi^4 + a_5\xi^5 \tag{7}$$

where

$S^* = w/x_0$ (flat plate)

w = cavity width

x_c = effective running length

$\xi = \log_{10}(S^*)$

$a_0 = 0.\overline{1}1706$

$a_1 = 0.088707$

$a_2 = -0.049822$

$a_3 = -0.0020116$

$a_4 = 0.0047757$

$a_5 = 0.0006549$

The expression for the local Stanton number is

$$St_y\, Re_L^{1/2} = \frac{c_1\left(\frac{v}{U_d}\right)^{c_2}}{\left[\int_0^{\frac{v}{L}} \left(\frac{v}{U_d}\right)^{c_3} d\left(\frac{v}{L}\right)\right]^{1/2}} \tag{8}$$

for air ($p_r = 0.7$), $c_1 = 0.418$, $c_2 = 0.435$, $c_3 = 1.87$ and the dividing streamline temperature T_d is found from Schlichting.[11]

$$T_d = T_c + \left(\frac{U_d}{U_e}\right) (T_{aw} - T_c) - \left(\frac{U_d}{U_e}\right)^2 \gamma \frac{U_e^2}{2c_p} \tag{9}$$

The cavity temperature was assumed as

$$T_c = 0.5 \ (T_d + T_w) \tag{10}$$

eliminate T_c from Eq. (9) and (10), expression of T_d is

$$T_d = \frac{\frac{1}{2} T_w + (T_{ad} - \frac{1}{2} T_w) \frac{U_d}{U_e} - \gamma \left(\frac{U_d}{U_e}\right)^2 \frac{U_e^2}{2c_p}}{\frac{1}{2} \left(1 + \frac{U_d}{U_e}\right)} \tag{11}$$

The reattachment zone length L was given by Nester,[12]

$$L = L_i \frac{1 + .447 \frac{\gamma-1}{2} M_e^2}{5.22 + 4.41 \left(\frac{T_w}{T_e} - 1\right)} \tag{12}$$

where L_i is the value corresponding to incompressible flow,

$$L_i = 11.8 \frac{w}{R_{e_w}^{1/2}} \tag{13}$$

with above formulas, the heat transfer rate h is given by:

$$h = \frac{St_y V c_p \rho (T_d - T_w)}{(T_o - T_w)} \tag{14}$$

The above model and formulas (except Eq. (11)) were obtained from Hodgson's theory for a two-dimensional rectangular cavity. In order to apply this theory to predict the heat transfer rate in the central plane of axially-symmetric nozzle, simple modifications based upon empirical data were made, leading to the following formulae:

$$\left(\frac{Y}{a}\right)_m = \frac{Y}{a} + 0.05 \tag{15}$$

$$\left(\frac{h}{h_{ref}}\right)_m = .5\frac{h}{h_{ref}} \tag{16}$$

Equation (15) accounts for the flow reattaching inside the cavity instead of reattaching right at the corner, as in 2-D theory. Equation (16) describes the heat transfer to the cavity wall, strongly influenced by the horseshoe vortex within the cavity.

3.2 Zero Incidence Cases

A calculation, based on the above formula, was made to compare with AEDC test data as shown in Fig. 25. For zero incidence cases, this modified Hodgson's method matches AEDC test data pretty well. This strongly indicates that the flow before the cavity was laminar during the test of zero incidence cases. This could happen because during the test of zero incidence cases, a slightly negative angle of attack was made to compensate for the displacement effect of the boundary layer. And since the growth of boundary layer is non-linear, by doing this compensation

the boundary layer would tend to be stabilized because of a slightly favorable pressure gradient away from the leading edge. Hence, in spite of the high Reynold's number in the test condition, the flow may well be stabilized sufficiently that the onset of transition occurs downstream of the cavity.

3.3 Angle of Attack Cases

In Fig. 27, in the angle of attack cases, there is an order of magnitude increase in the normalized experimental heat transfer rate above the zero angle of attack results. This increased heating is not predicted by the model described above. In order to find the reason for this order of magnitude discrepancy, several lines of study were followed:

(a) External Flow Properties - The pressure data showed that there was a weak shock ahead of the first point of the test data, which was 7.65" from the center of the cavities. This shock might be due to the junction of the test plate with the leading edge. This junction was 8.76" from the center of cavity. But calculation showed that this weak shock did not have much influence on the external flow in the vicinity of the cavity and would not thereby effect reattachment wall heating rate.

(b) The plot of actual heat transfer rate, Fig. 28, showed that the order of magnitude discrepancy was in the actual heat transfer rate and not due to a poor choice of h_{ref}.

(c) Since the parameter which characterized the Hodgson's theory is the velocity along the dividing streamline, a calculation, which did

not include the empirical factor of 0.5 in Eq. (16), based on the assumption of laminar flow ahead of the cavity but with increased dividing streamline velocity, which corresponding the maximum heat transfer rate, was carried out. The results, Fig. 29, are comparable to the test data.

(d) Since in the test data there was no clear indication of whether the flow before the cavity was laminar or turbulent, a calculation of the heat transfer rate in the central plane based on the assumption of turbulent boundary layer ahead of the cavity was also carried out. The dividing streamline velocity in the turbulent shear layer was given by Lamb.[14]

The results of this calculation are shown in Fig. 30. These results were about the same as that of the maximum rate possible in laminar flow as calculated in part (c) and were comparable to the test data. It should be noted that in this calculation only the dividing streamline velocity was calculated for a turbulent shear layer, whereas both the velocity in recompression zone (See Fig. 24) and the local Stanton number were still calculated by using laminar flow equations. It is also worth noting that only a change of laminar boundary layer to turbulent boundary layer before the cavity has brought the heat transfer rate to the maximum possible value in laminar flow. This reveals the importance of the study of turbulent flow. Hence, a more thorough study based on the consistent turbulent flow is needed for future work.

RESULTS

Several conclusions may be drawn from the preceding discussion:

1. The boundary layer-cavity interaction generates a horseshoe vortex reminiscent of the vortex system of a wing of finite span.
2. The pressure distribution in and around the cavity is influenced very strongly by this horseshoe vortex. The influence of this vortex will extend far downstream, and laterally beyond the sides of the cavity.
3. Bleeding cold gas through the nozzle increases the strength of the vortex and, consequently, increases the peak heating rate in the nozzle.
4. The key to passive system heat protection in the region of the cavity is the control of the vortex strength by shaping of the nozzle. Variation of cavity geometry could tend to weaken the vortex, thereby relieving the heating problem.
5. For zero incidence cases, the method modified from 2-D laminar theory gives good prediction in the central plane of axially-symmetric nozzle.
6. For angle of attack cases, based on the assumption of turbulent boundary layer ahead of the cavity, the prediction of heat transfer rate is comparable to AEDC test data.

7. The heat transfer rate on the reattachment wall calculated based on the turbulent velocity profile was an order of magnitude higher than that calculated based on laminar flow.

REFERENCES

1. -- Test Facilities Handbook (Ninth Edition), Arnold Engineering Development Center, Tennessee (July 1971).

2. Hermann, R., Hypersonic Aerodynamic Problems at Re-entry of Space Vehicles, UARI Res. Report No. 29, University of Alabama Research Institute, Huntsville, Alabama (November 1965).

3. -- Space Shuttle Altitude Control System (ACS) Thrustor Penetration Heating, Second Quarterly Progress Report, Contract NAS8-27683, for NASA-MSFC; Report No. 632-TP-3, General Dynamics/Convair Aerospace Division, San Diego (January 1972).

4. Robinson, A. and Laurmann, J. A., Wing Theory , Cambridge Univ. Press, (1953).

5. Burggraf, O.R., "A Model of Steady Separated Flow in Rectangular Cavities at High Reynold's Number", Proc. 1965 Heat Transf. and Fluid Mech. Inst., (A. F. Charwat, ed.) Stanford Univ. Press, pp. 190-229 (1965).

6. Hodgson, J. W., "Heat Transfer in Separated Laminar Hypersonic Flow," AIAA Journal, Vol. 8, No. 12, pp. 2291-2293 (December 1970).

7. Thomke, G. J., Separation and Reattachment of Supersonic Turbulent Layer Behind Downstream Facing Steps and Over Cavities, Report No. SM-43602, STAR Accession No. N64-22007, Douglas Airc., Santa Monica, Calif. (1964).

8. Chung, P. M. and Viegas, J. R., "Heat Transfer at Reattachment Zone of Separated Laminar Boundary Layers", TN D1072, NASA, 1961.

9. Denison, M. R. and Baum, E., "Compressible Free Shear Layer with Finite Initial Thickness", AIAA J., Vol. I, No. 2, pp. 342-349, 1963.

10. Engel, C. D., "The Propulsive Altitude Control System - An Open Cavity Heating Problem", Remtech Incorporated, RTR 008-1, April 1972.

11. Schlichting, H., "Boundary-Layer Theory, 6th Ed., pp. 322, McGraw-Hill, New York, 1968.

12. Nestler, D. E., Laminar Heat Transfer to Cavities in Hypersonic Low Density Flow", Proceedings of the Third International Heat Transfer Conference, American Society of Mechanical Engineers, Vol. II, pp. 251-261, 1966.

13. Nicoll, K. M., "A Study of Laminar Hypersonic Cavity Flows", AIAA Journ., Vol. 2, No. 9, pp 1535 ~ 1541 (September 1964).

14. Lamb, J. P., "An Approximate Theory for Developing Turbulent Free Shear Layers", J. of Basic Engineering, Trans. of ASME, pp. 633-642, (September 1967).

Table I. Wind Tunnel Operating Conditions From

AEDC VKF Tunnel B

Mach No.	Stagnation Pressure N/m^2 (lb/in^2)	Stagnation Temp. ^oK (^oR)	Static Temp. ^oK (^oR)	Static Press. N/m^2 (lb_f/in^2)	Freestream Density kg/m^3 ($slug/ft^3$)	Reynolds No. $10^6/m$ ($10^6/ft$)	Freestream Velocity m/sec (ft/sec)
7.895	8.963×10^5 (130)	672.2 (1210)	50.0 (90)	96.53 (.014)	$.224 \times 10^{-3}$ (1.399×10^{-5})	2.296 (.7)	1117 (3665)
7.968	28.958×10^5 (420)	716.7 (1290)	52.2 (94)	303.37 (.044)	$.647 \times 10^{-3}$ (4.04×10^{-5})	6.562 (2.0)	1152 (3780)
8.013	59.639×10^5 (965)	746.7 (1344)	53.9 (97)	599.84 (.087)	1.219×10^{-3} (7.615×10^{-5})	12.139 (3.7)	1180 (3870)

Table II. Flat Plate Flow Field Conditions in AEDC Test

Case No.	M_∞	T_∞ ^oR	P_∞ lb_f/in^2	U_∞ ft/sec	P_{oj} lb_f/in^2	T_{oj} ^oR	θ deg.	D_j in.
1	8.00	97.6	.089	3874	0	527	0.13	2
2	8.00	98.3	.089	3887	6.9	530	0.13	2
3	8.00	98.3	.089	3887	25.9	530	0.13	2
4	8.00	98.3	.089	3877	0	571	-0.08	1
5	8.00	97.8	.089	3877	0	573	-0.03	1/2
6	7.92	84.0	.014	3557	0	561	-0.08	2
7	8.00	97.8	.089	3877	0	606	9.95	2
8	8.00	97.8	.089	3876	0	627	27.97	2
9	8.00	97.8	.089	3877	0	593	9.95	1
10	8.00	98.1	.089	3882	0	618	27.97	1

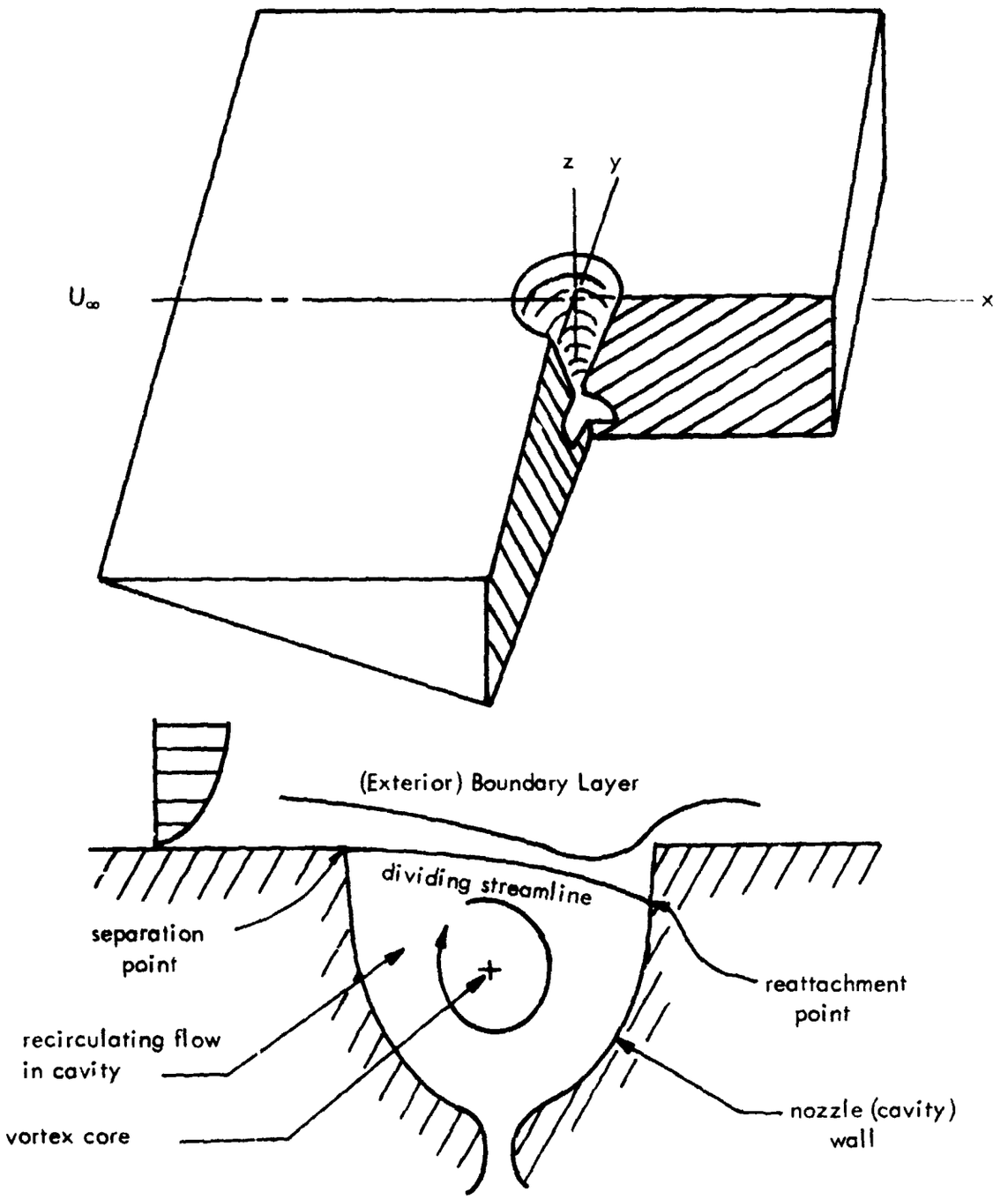

FIG. 1. Typical Installation of an Axially Symmetric Nozzle in a Flat Plate.

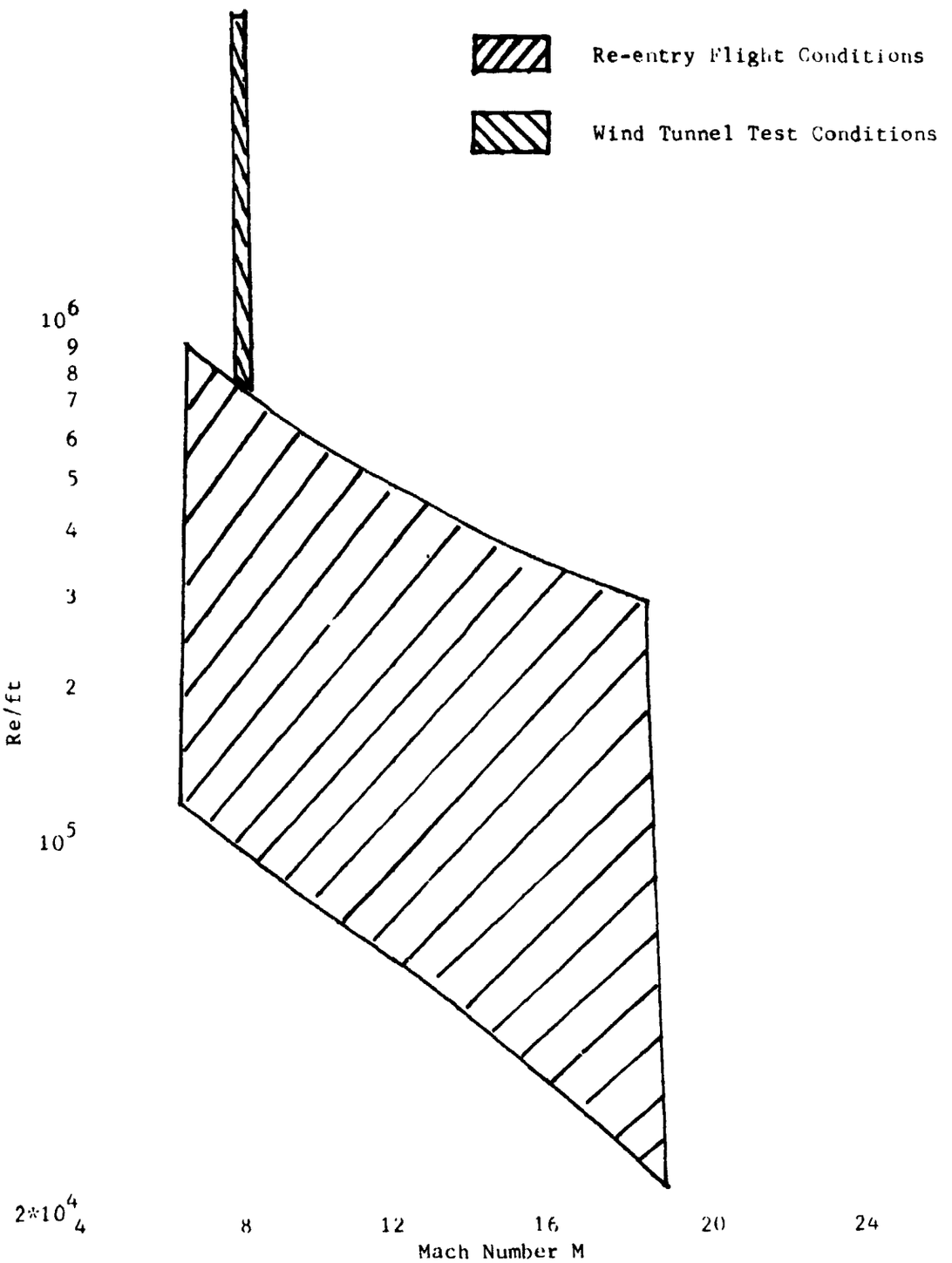

Fig. 2. Comparison of Mach Numbers between Re-entry Flight and Wind Tunnel Test Conditions

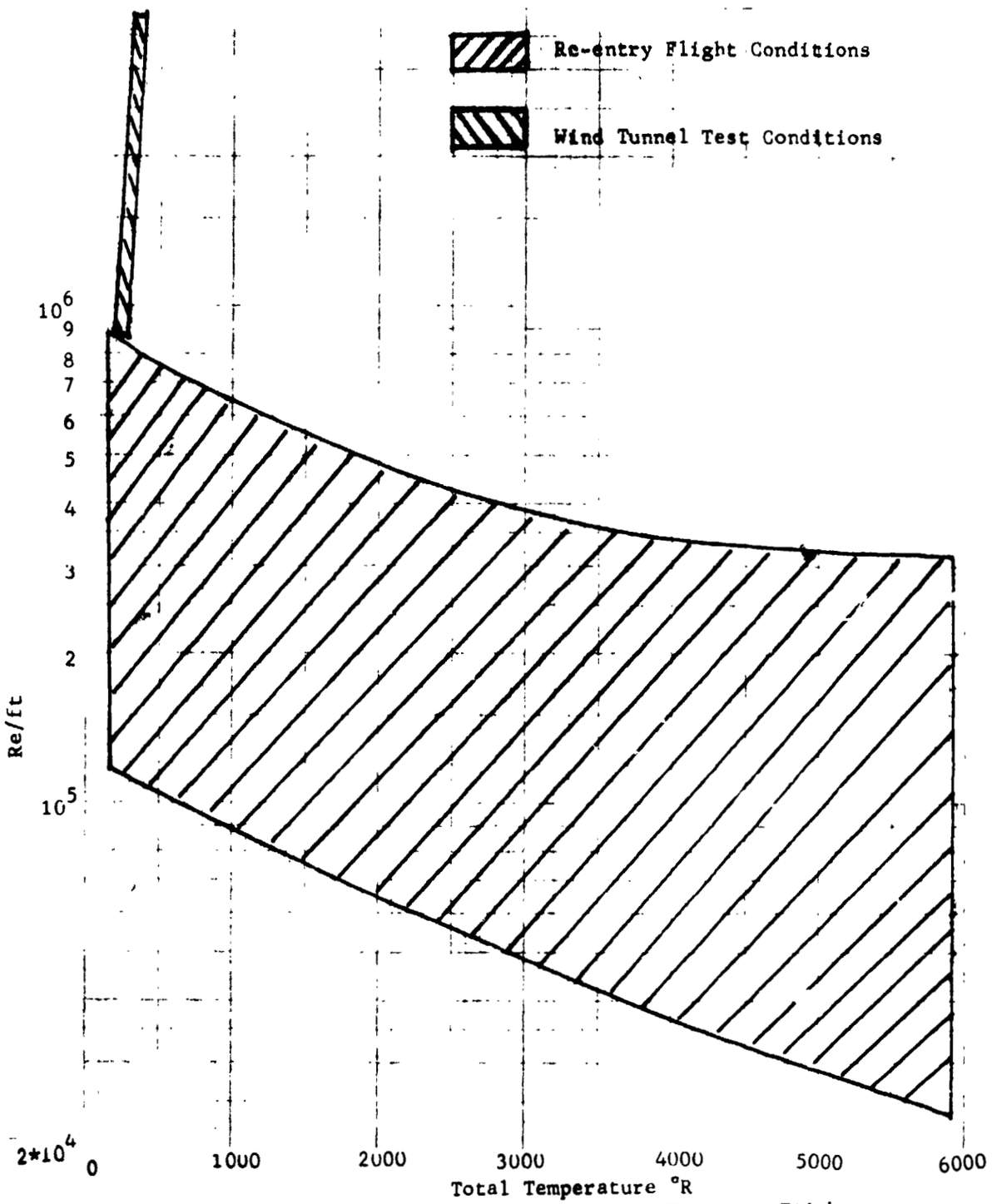

Fig. 3. Comparison of Total Temperature between Re-entry Flight and Wind Tunnel Test Conditions

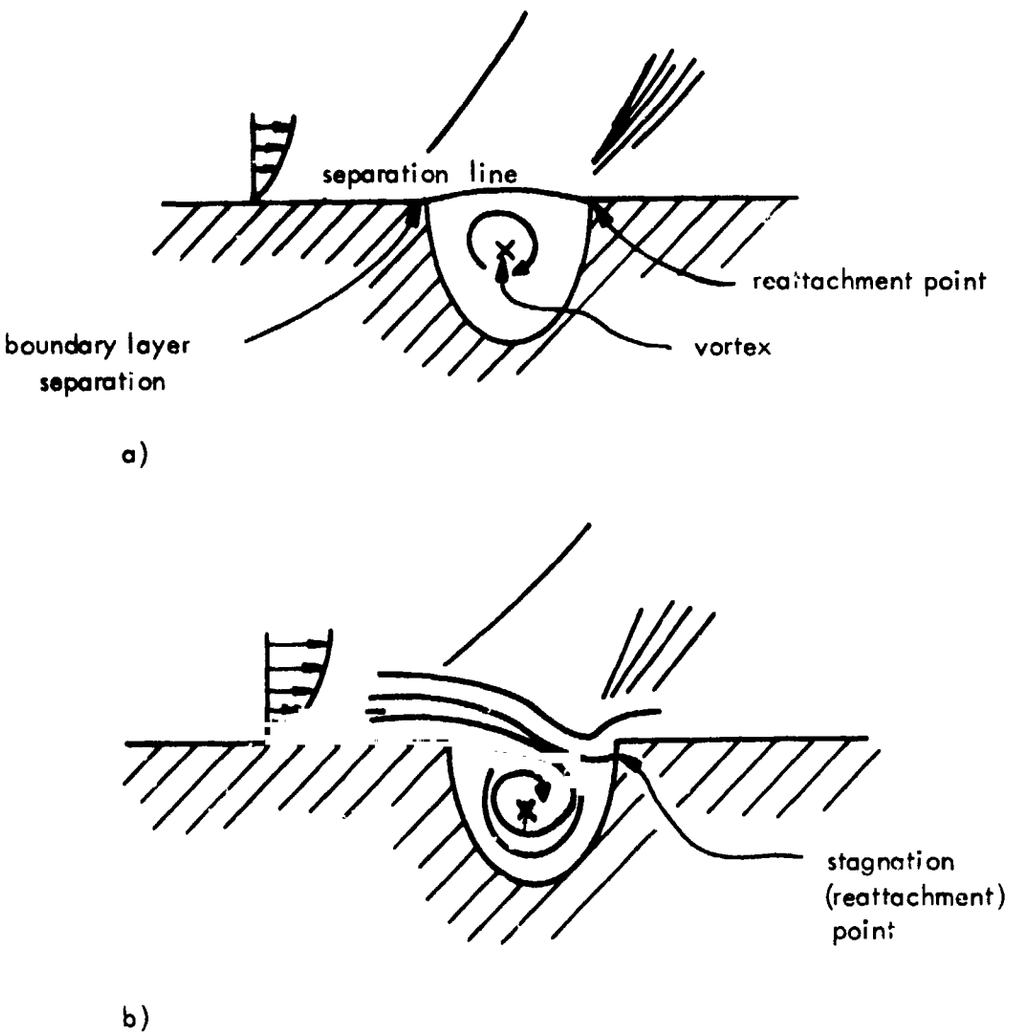

FIG. 4. Sketches of Flow in Cavity.

a) Two-dimensional Flow

b) Plane of Symmetry in 3-D Case

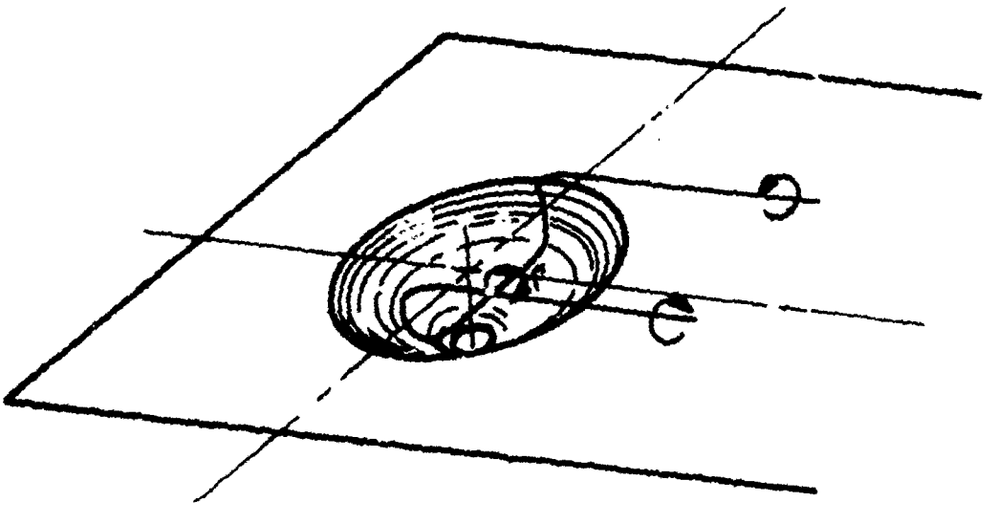

FIC. 5. Horseshoe Vortex for Three-Dimensional Cavity Flow.

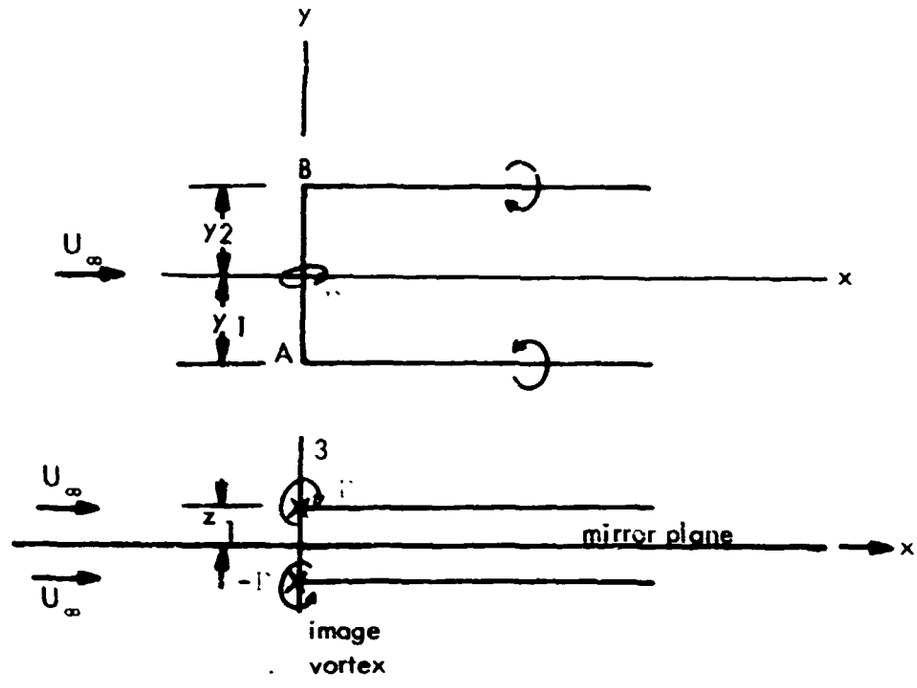

FIG. 6. Superposition of Horseshoe Vortex and Free Stream, Using Method of Images to Enforce no Flow Through the Surface.

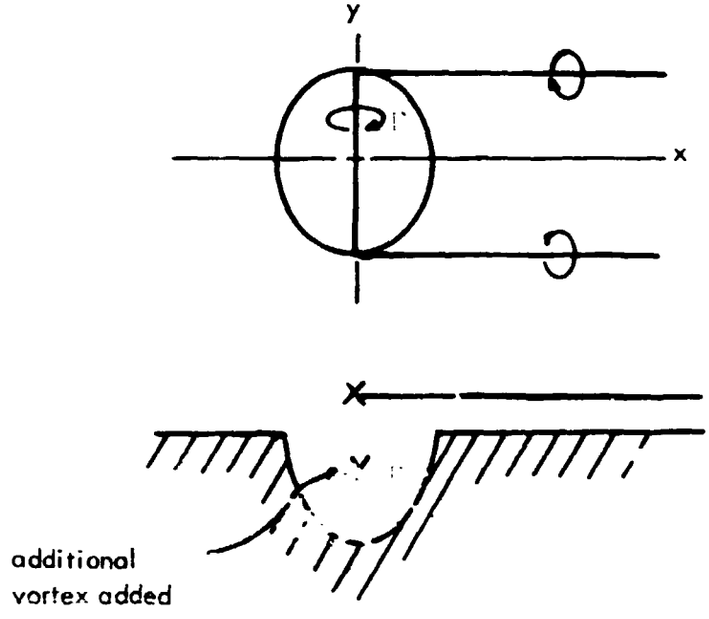

FIG. 7. Horseshoe Vortex Model With Additional Vortex Segment to Induce Flow Through Cavity Exit Plane.

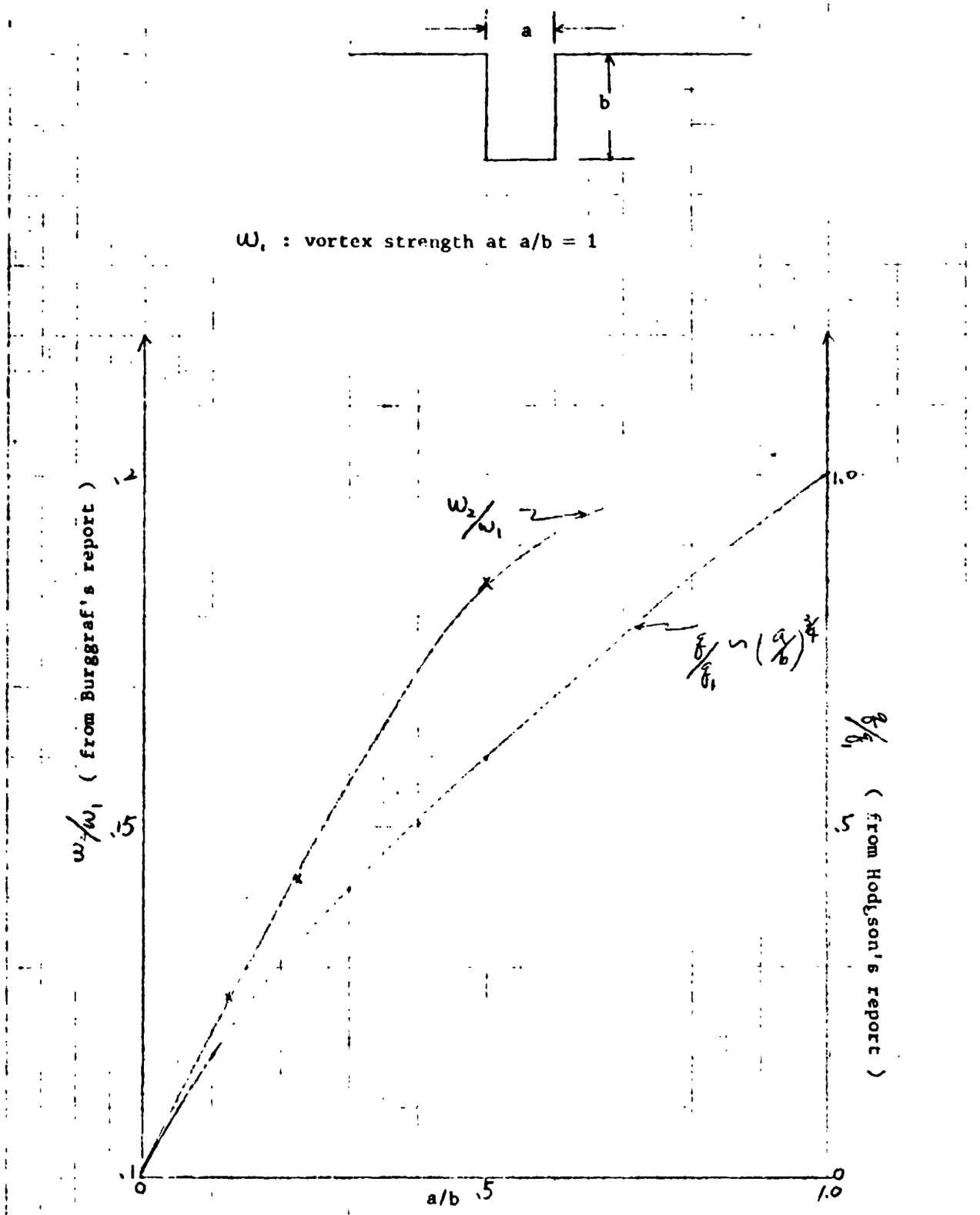

Fig. 8. Vortex strength and local heat transfer distribution with various cavity width, assuming constant cavity depth

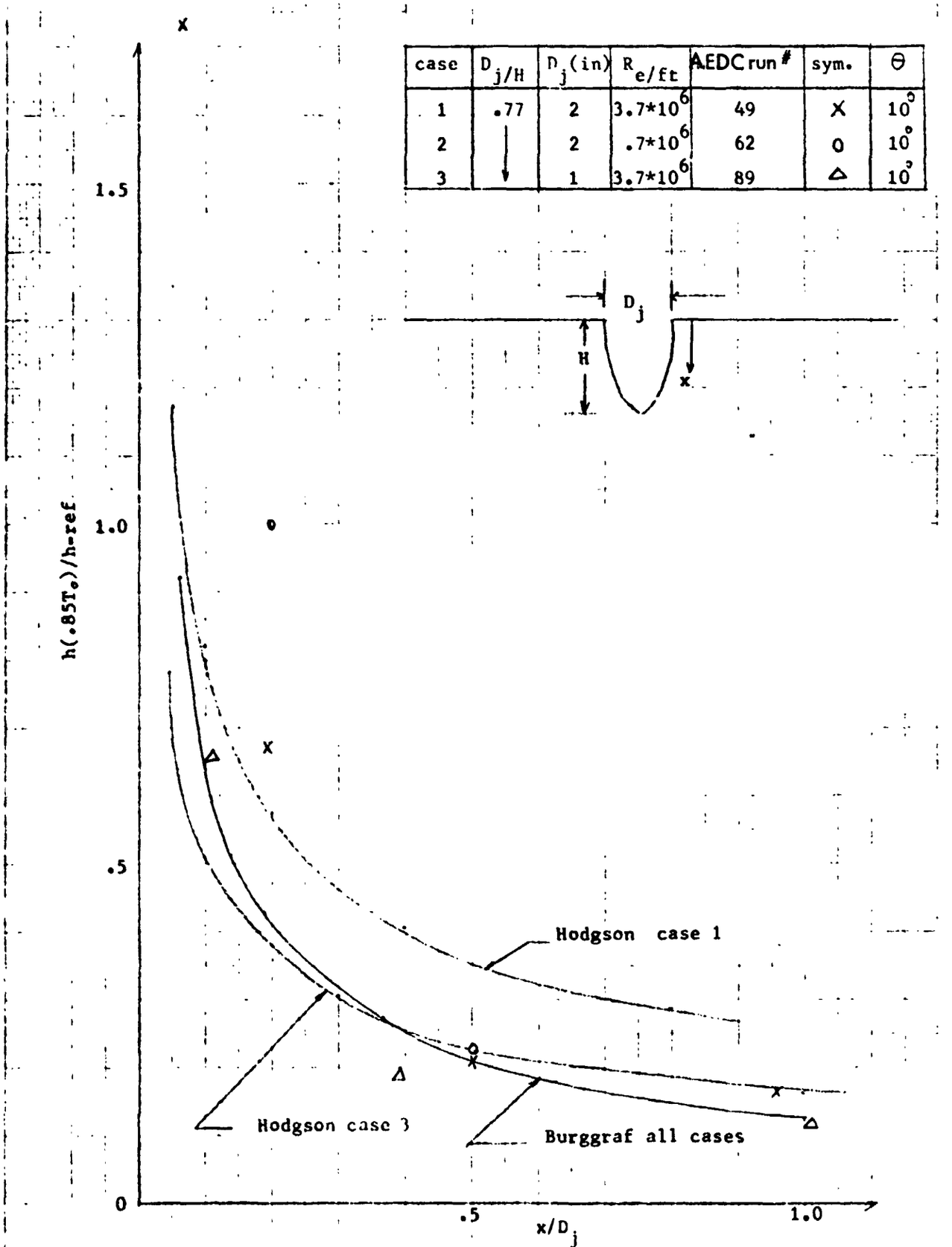

Fig. 9 COMPARISON BETWEEN CENTRAL PLANE REATTACHMENT WALL AND TWO DIMENSIONAL THEORIES, WHERE ANGLE OF ATTACK IS 0

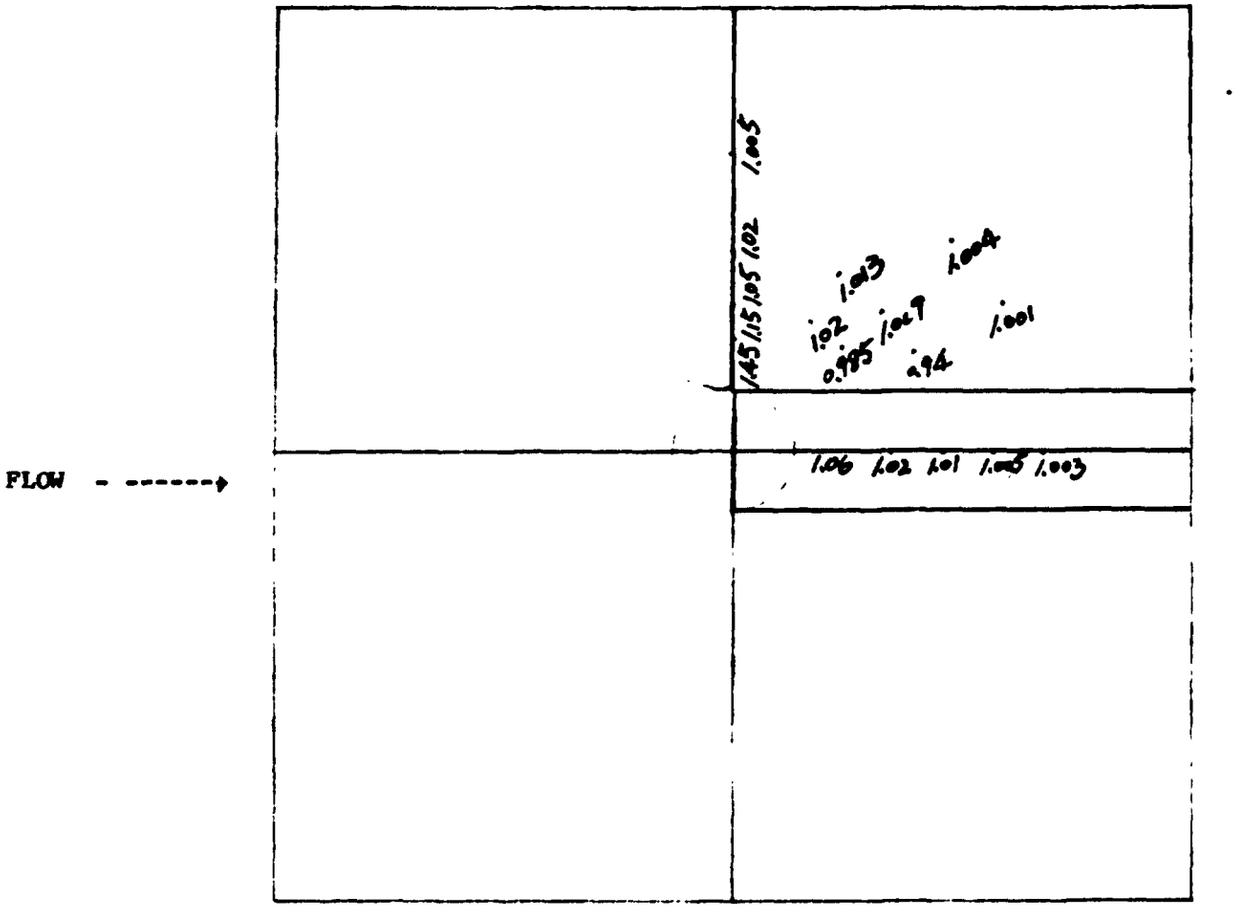

Fig. 10. PRIDICTED PRESSURE DISTRIBUTION BY HYDRODYNAMIC STUDY UNDER CASE 1

FLOW ---------▸

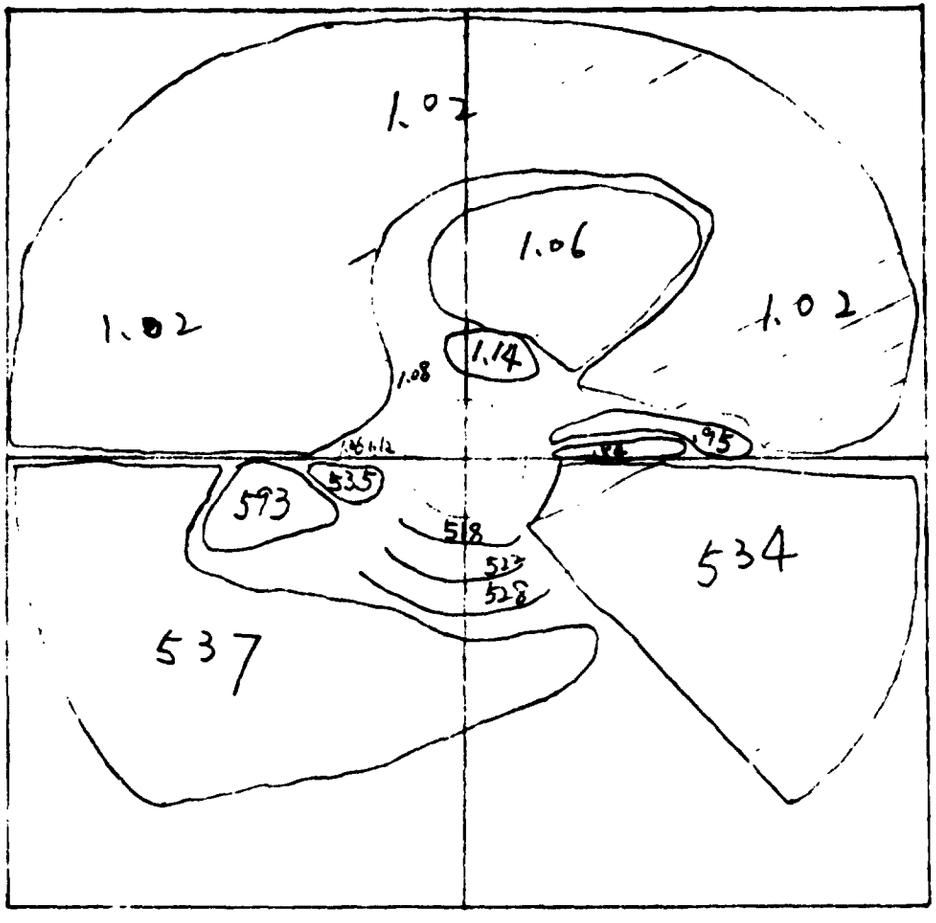

Fig. 11. ISOBAR (upper half, normalized by P-inf) AND ISOThERM °R (lower half) UNDER CASE 1

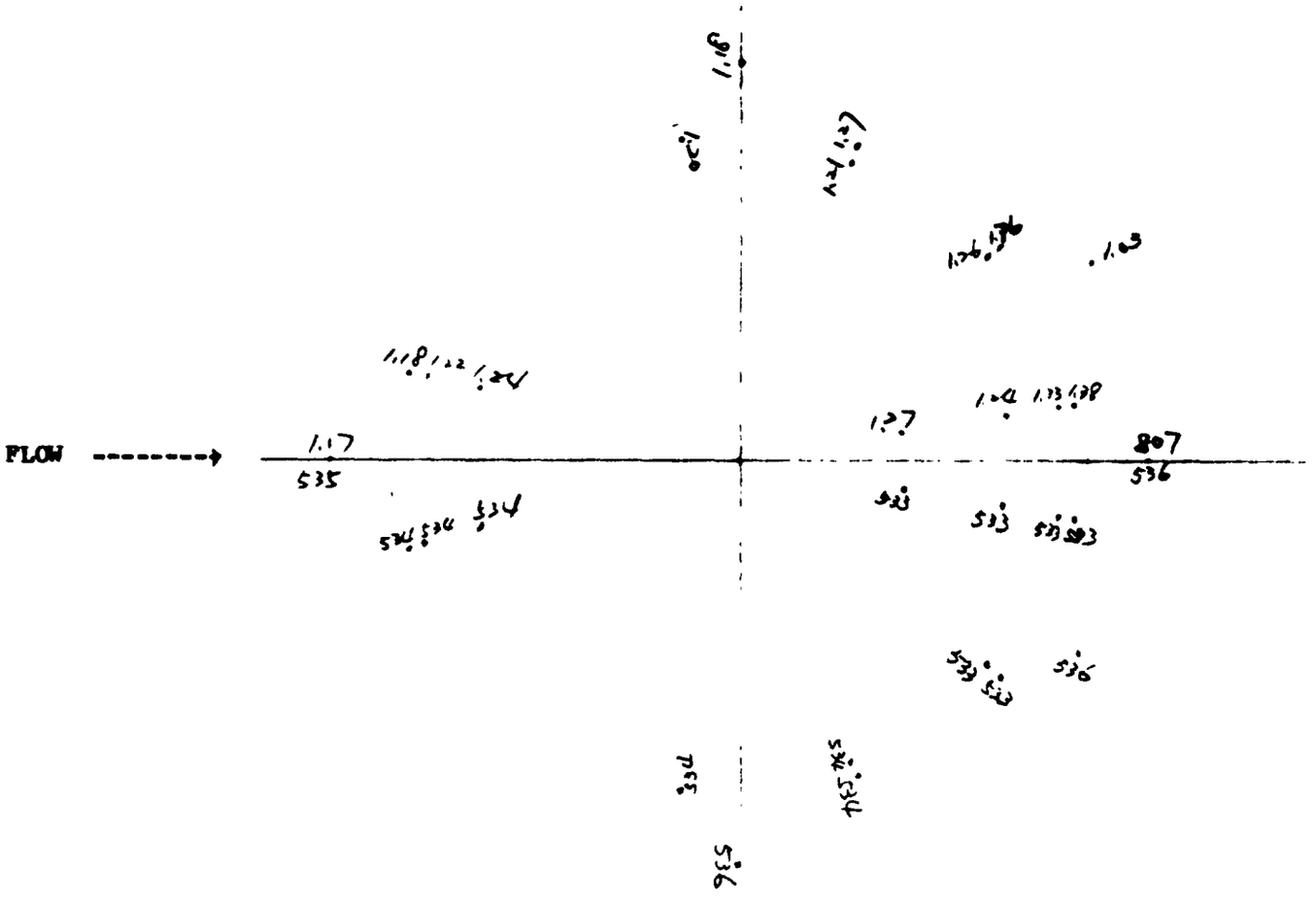

Fig. 12. PRESSURE (upper half, normalized by P-inf) AND TEMPERATURE (lower half, °R) DISTRIBUTIONS INSIDE AND AROUND THE EDGE OF CAVITY, UNDER CASE 1

FLOW ------->

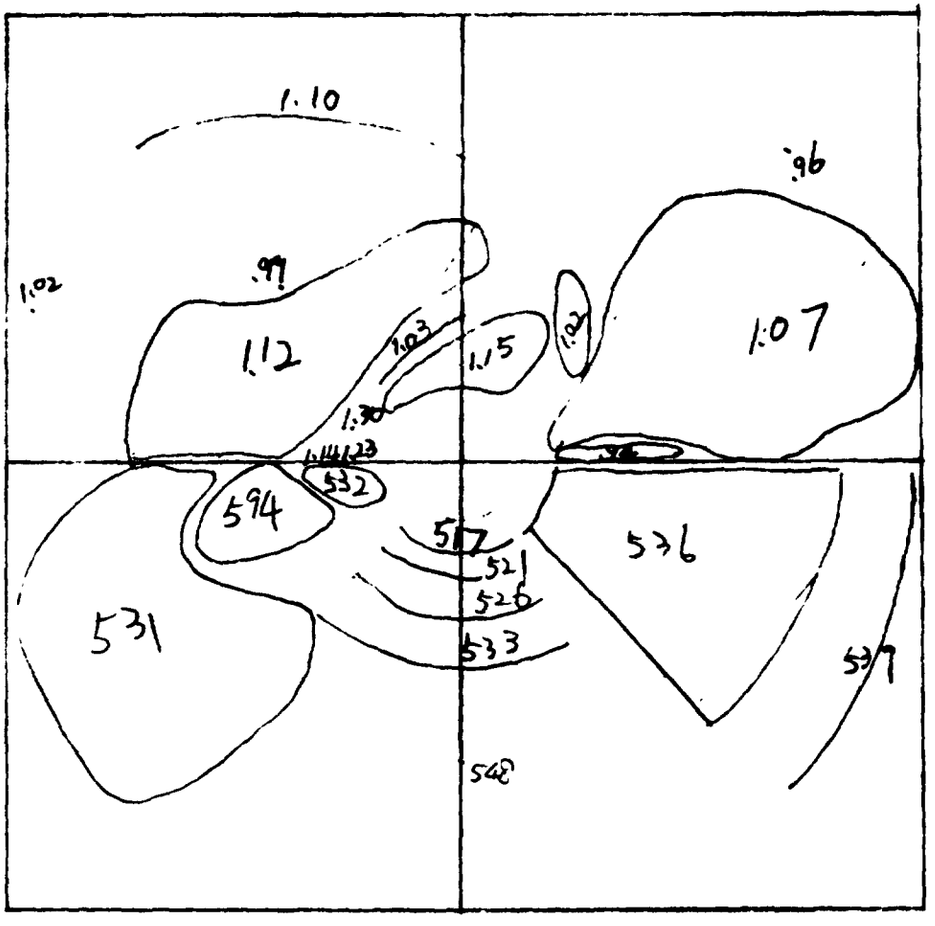

Fig. 13. ISOBAR (upper half, normalized by P-inf) AND ISOTHERM ^{o}R (lower half) UNDER CASE 2

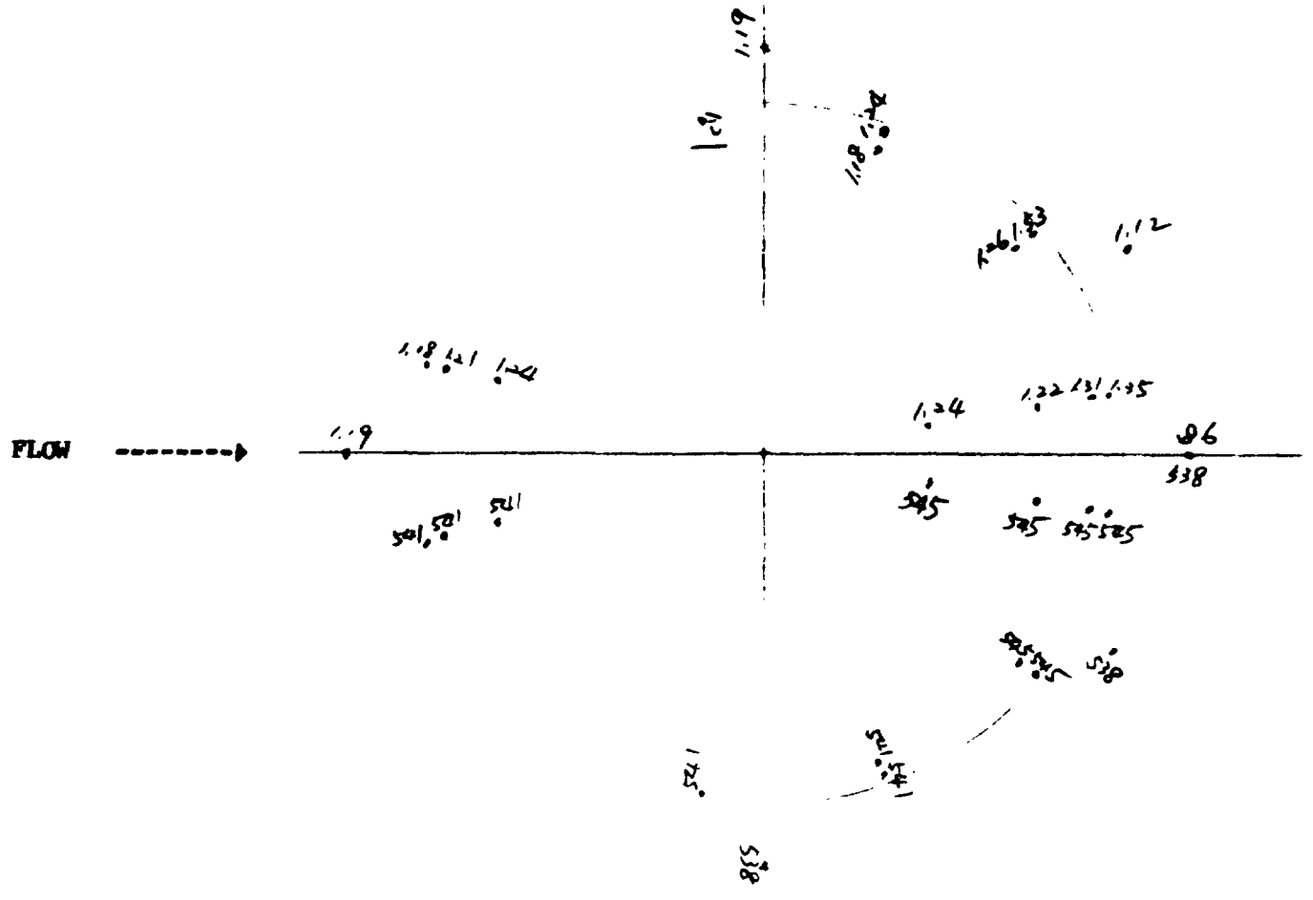

Fig. 14. PRESSURE (upper half, normalized by P-inf) AND TEMPERATURE (lower half, °R) DISTRIBUTIONS INSIDE AND AROUND THE EDGE OF CAVITY, UNDER CASE 2

FLOW ---------->

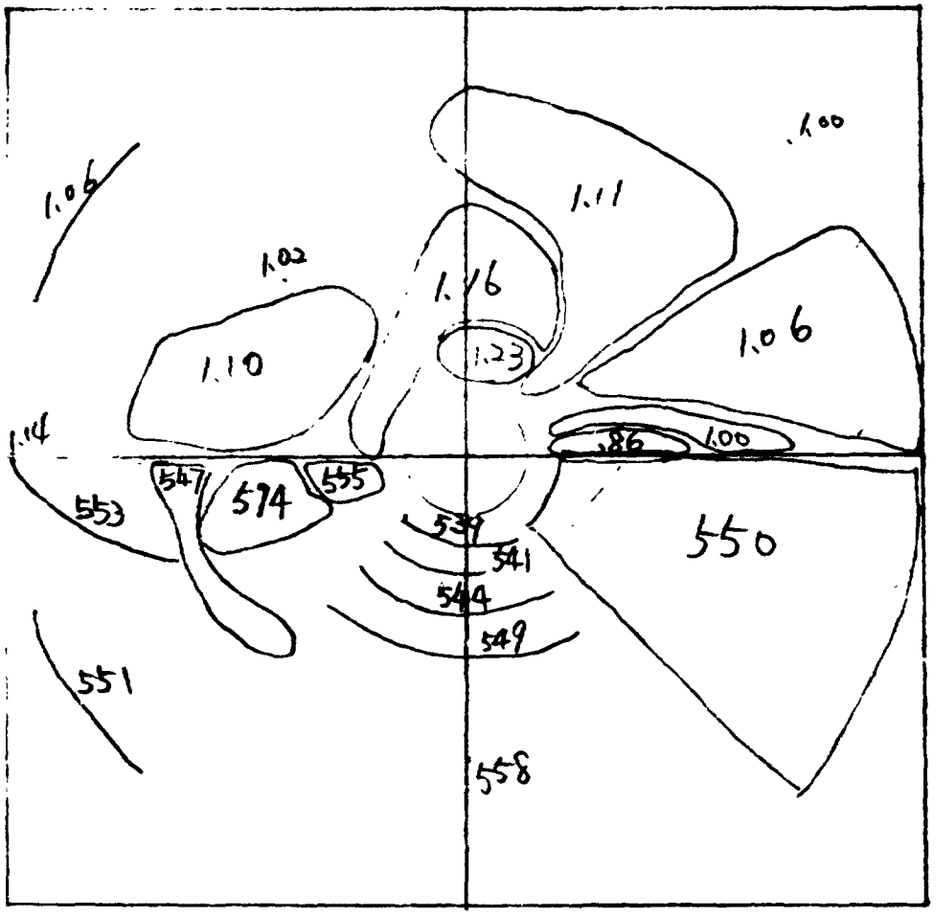

Fig. 15. ISOBAR (upper half, normalized by P-inf) AND ISOTHERM °R (lower half) UNDER CASE 3

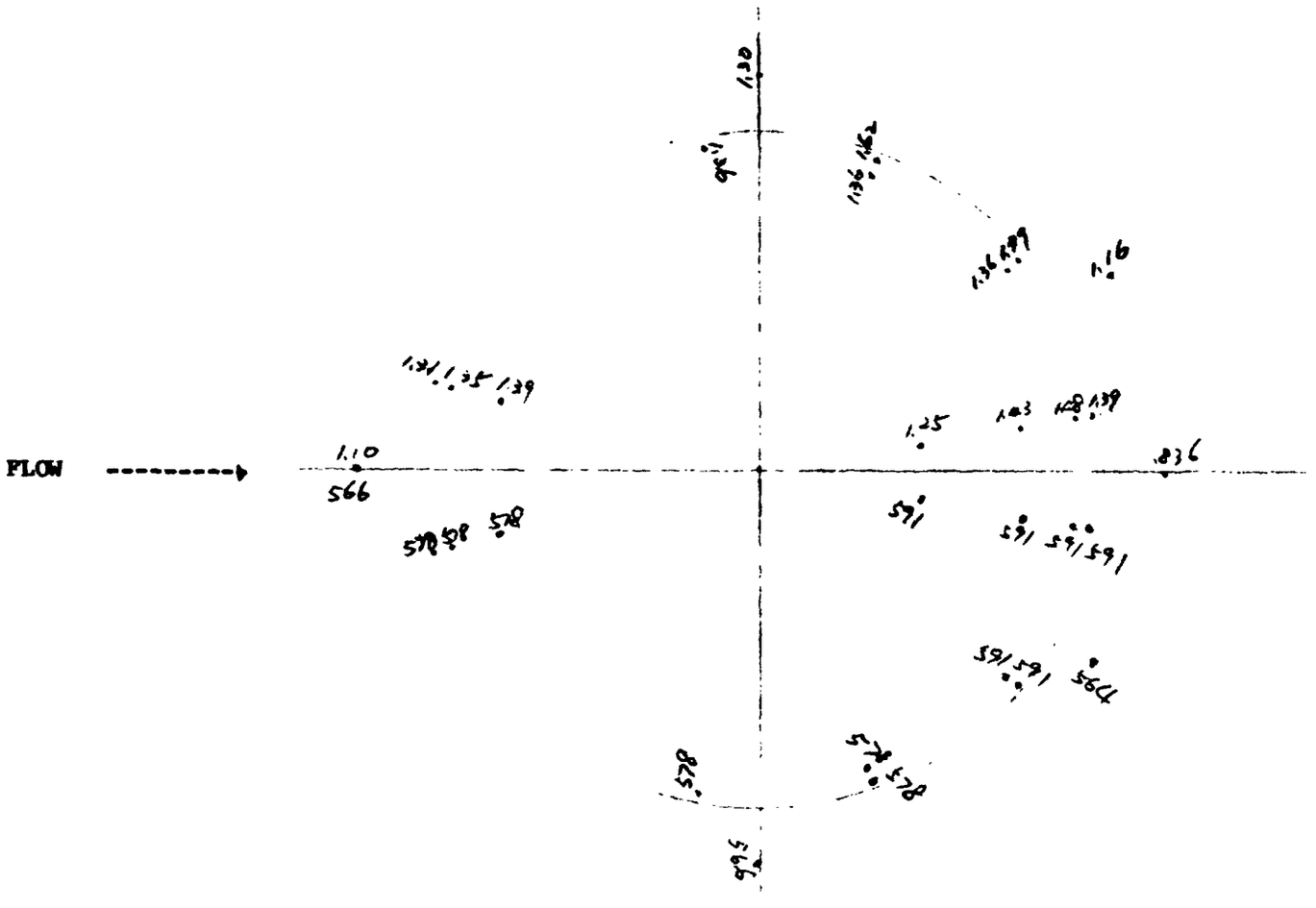

Fig. 16. PRESSURE (upper half, normalized by P-inf) AND TEMPERATURE (lower half, °R) DISTRIBUTIONS INSIDE AND AROUND THE EDGE OF CAVITY, UNDER CASE 3

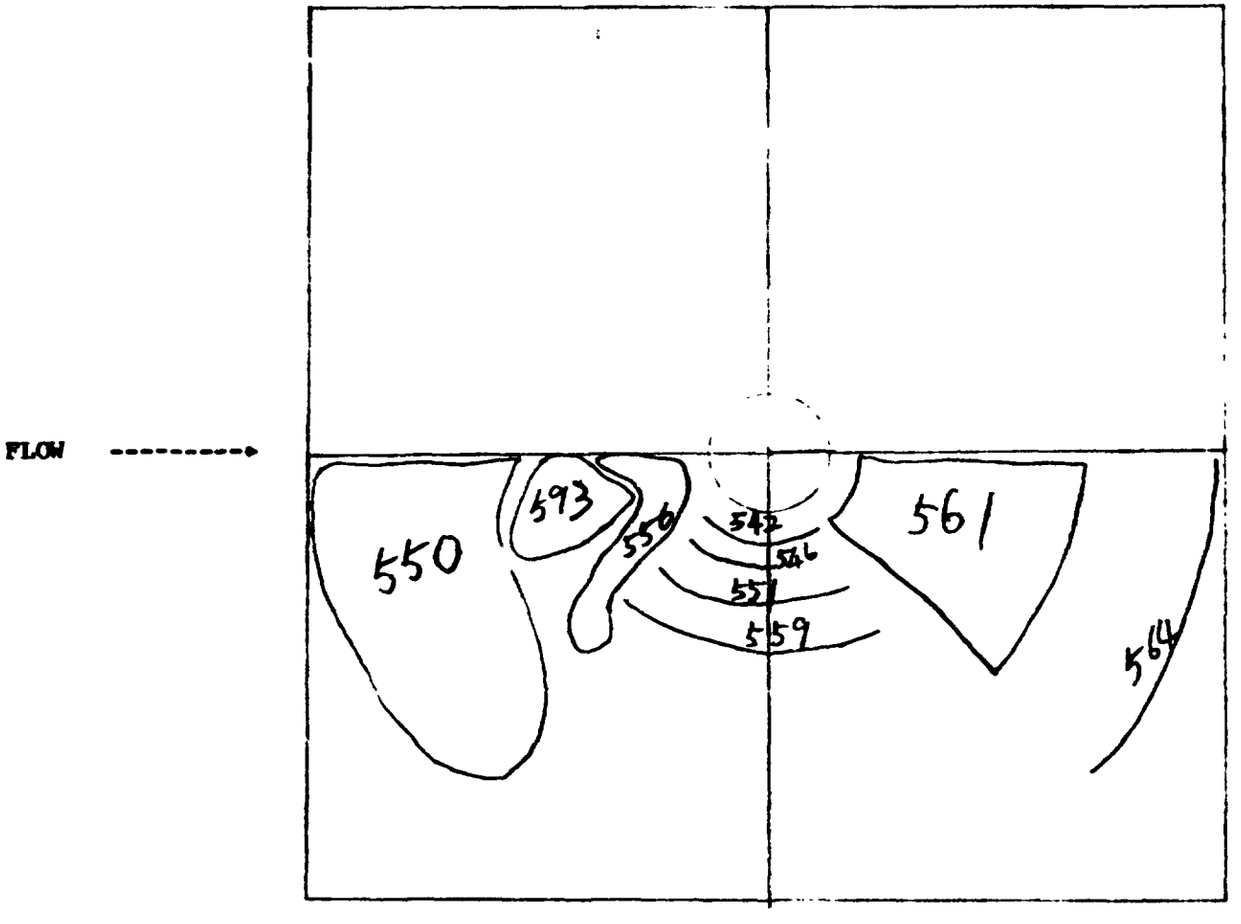

Fig. 17. ISOTHERMAL ZONES °R UNDER CASE 4

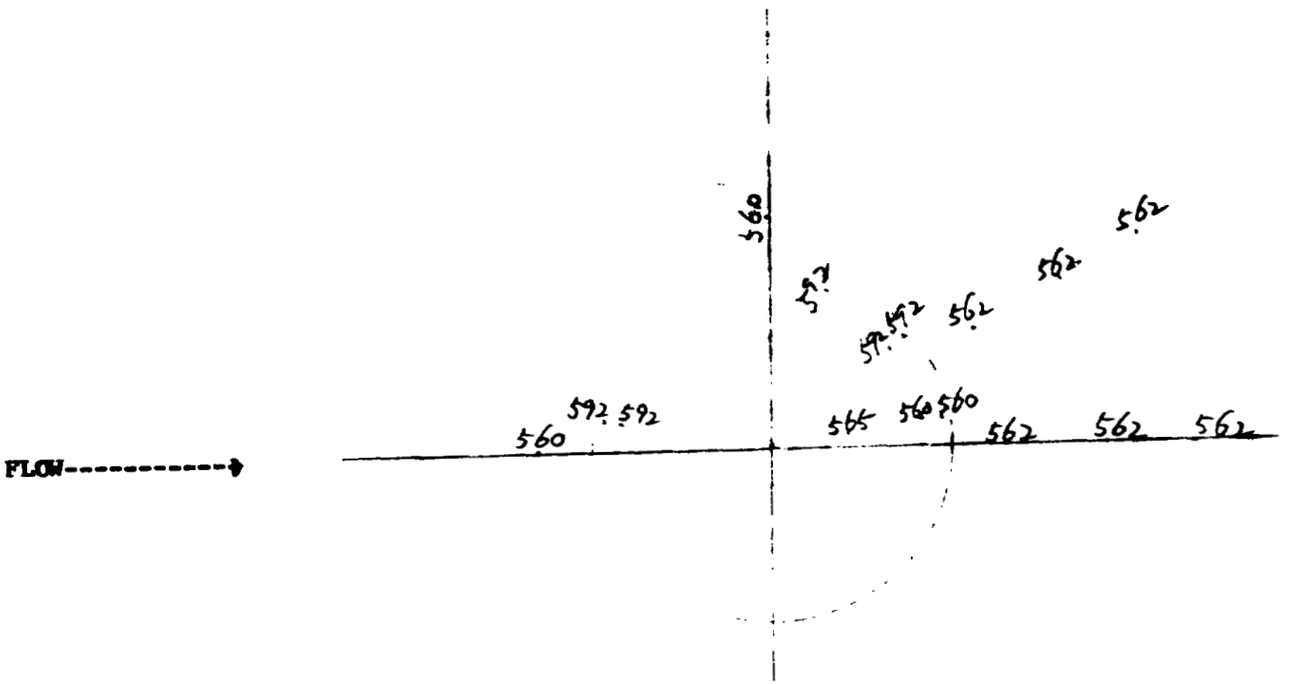

Fig. 18. TEMPERATURE DISTRIBUTION (°R) INSIDE AND AROUND THE EDGE OF THE CAVITY, UNDER CASE 4

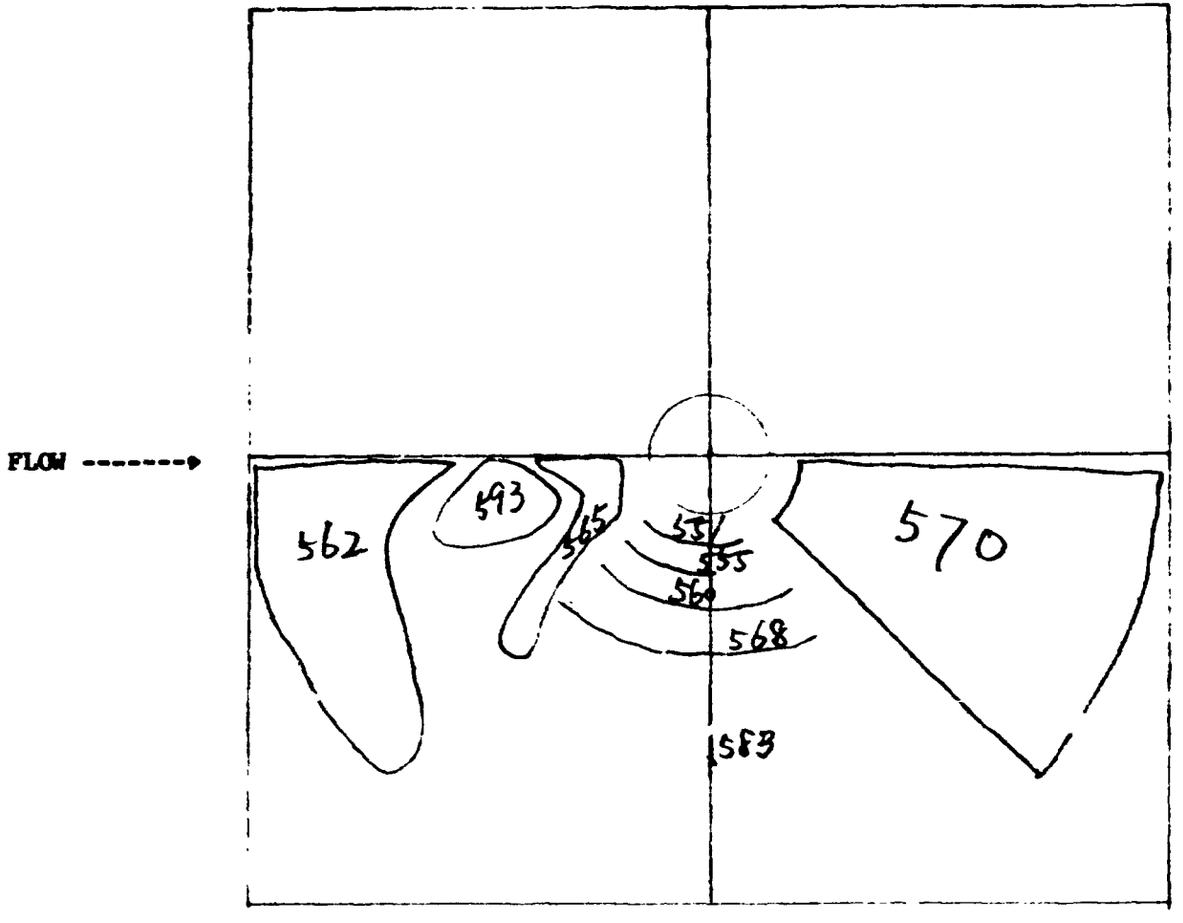

Fig. 19. ISOTHERMAL ZONES °R UNDER CASE 5

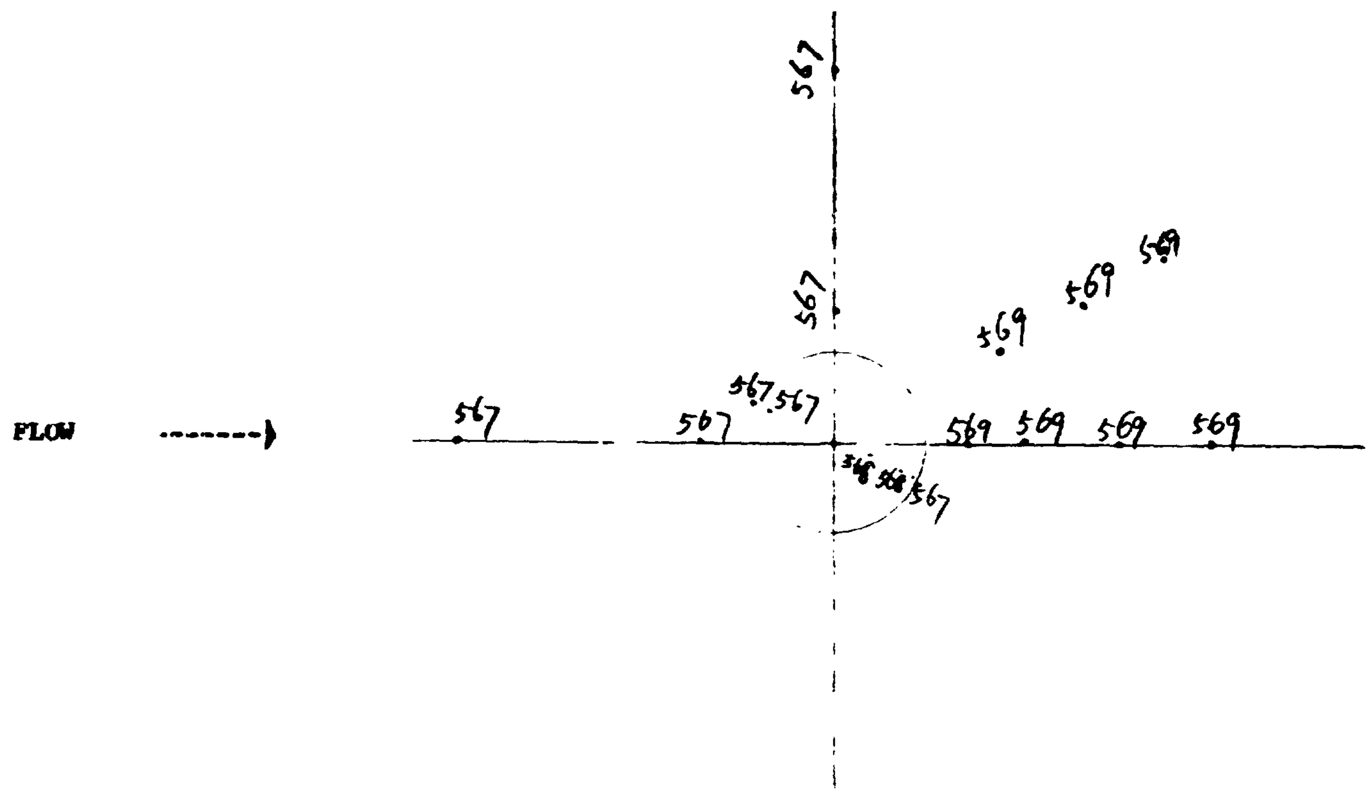

Fig. 20. TEMPERATURE DISTRIBUTION (°R) INSIDE AND AROUND THE EDGE OF THE CAVITY, UNDER CASE 5

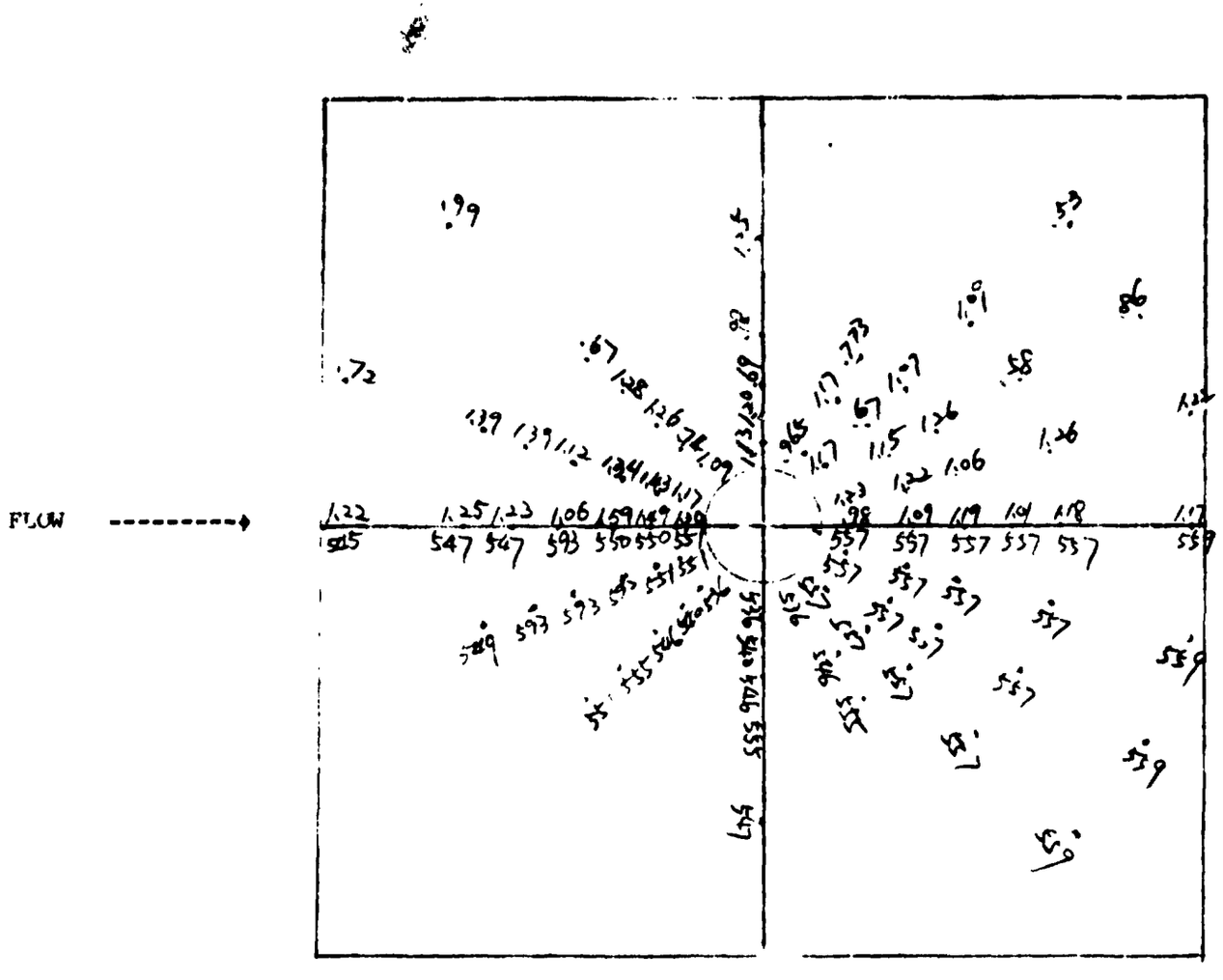

Fig. 21. PRESSURE DISTRIBUTION (upper half, normalized by P-inf) AND TEMPERATURE DISTRIBUTION °R (lower half) UNDER CASE 6

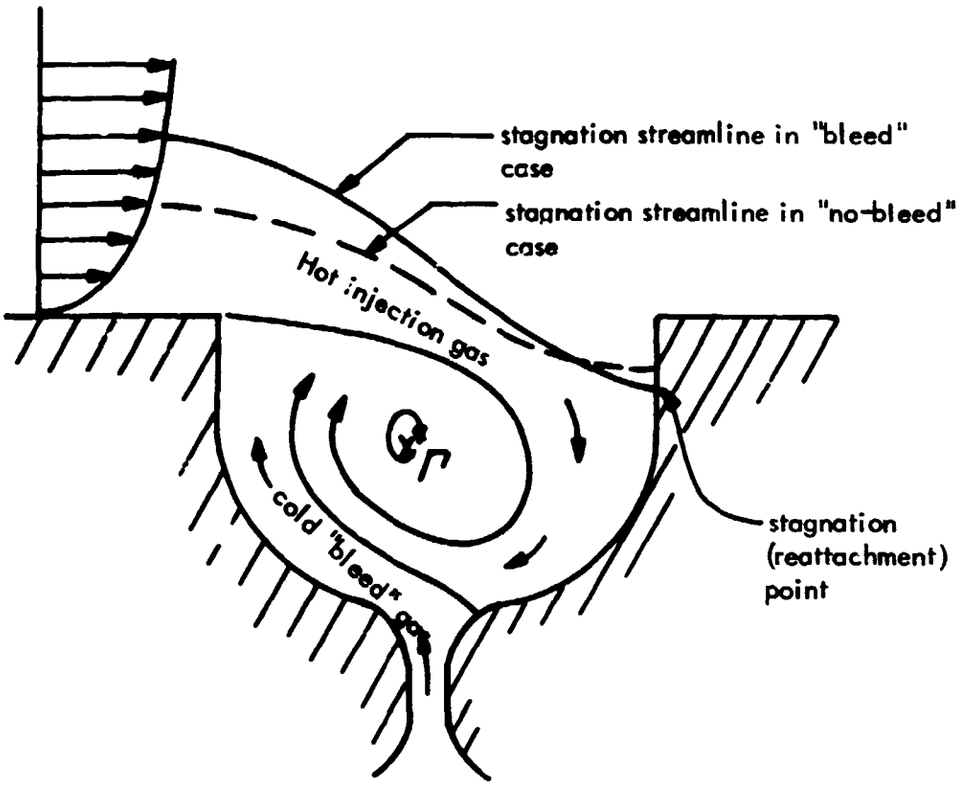

FIG. 22. Sketch of the Influence of Nozzle "Bleed" on the Flow in the Thrustor Cavity.

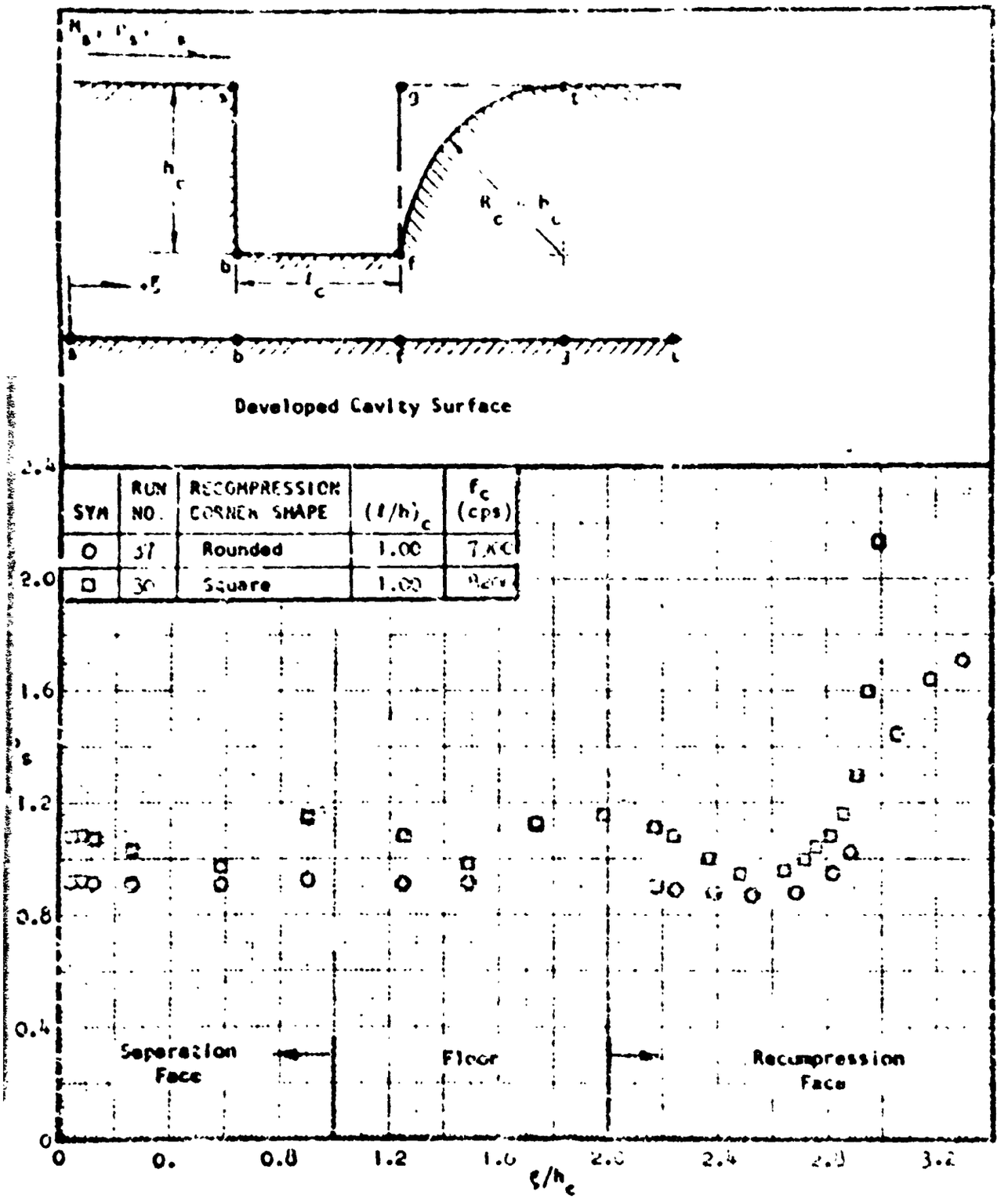

COMPARISON OF CAVITY WALL PRESSURE DISTRIBUTION OBTAINED FOR TWO RECOMPRESSION CORNER SHAPES. M_∞ = 2.09

TAKEN FROM REF.

FIGURE 23

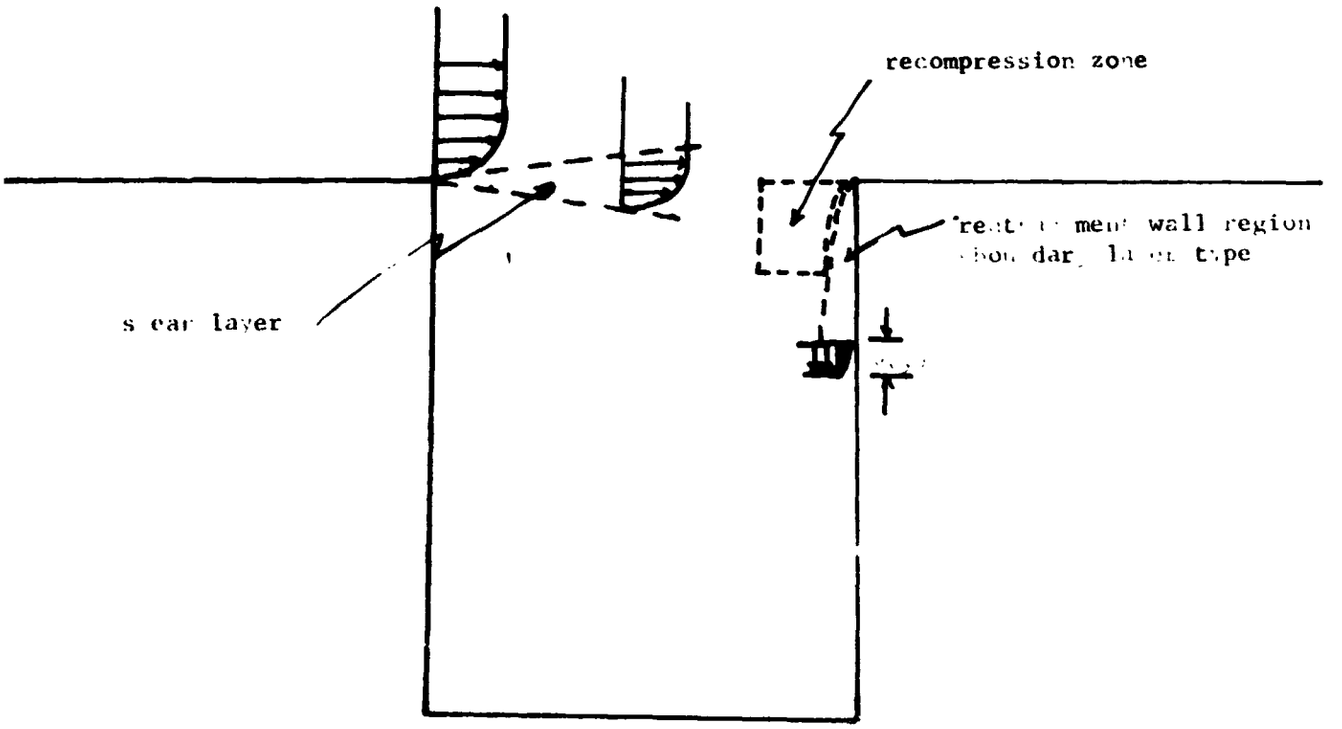

Fig. 24 Flow odel

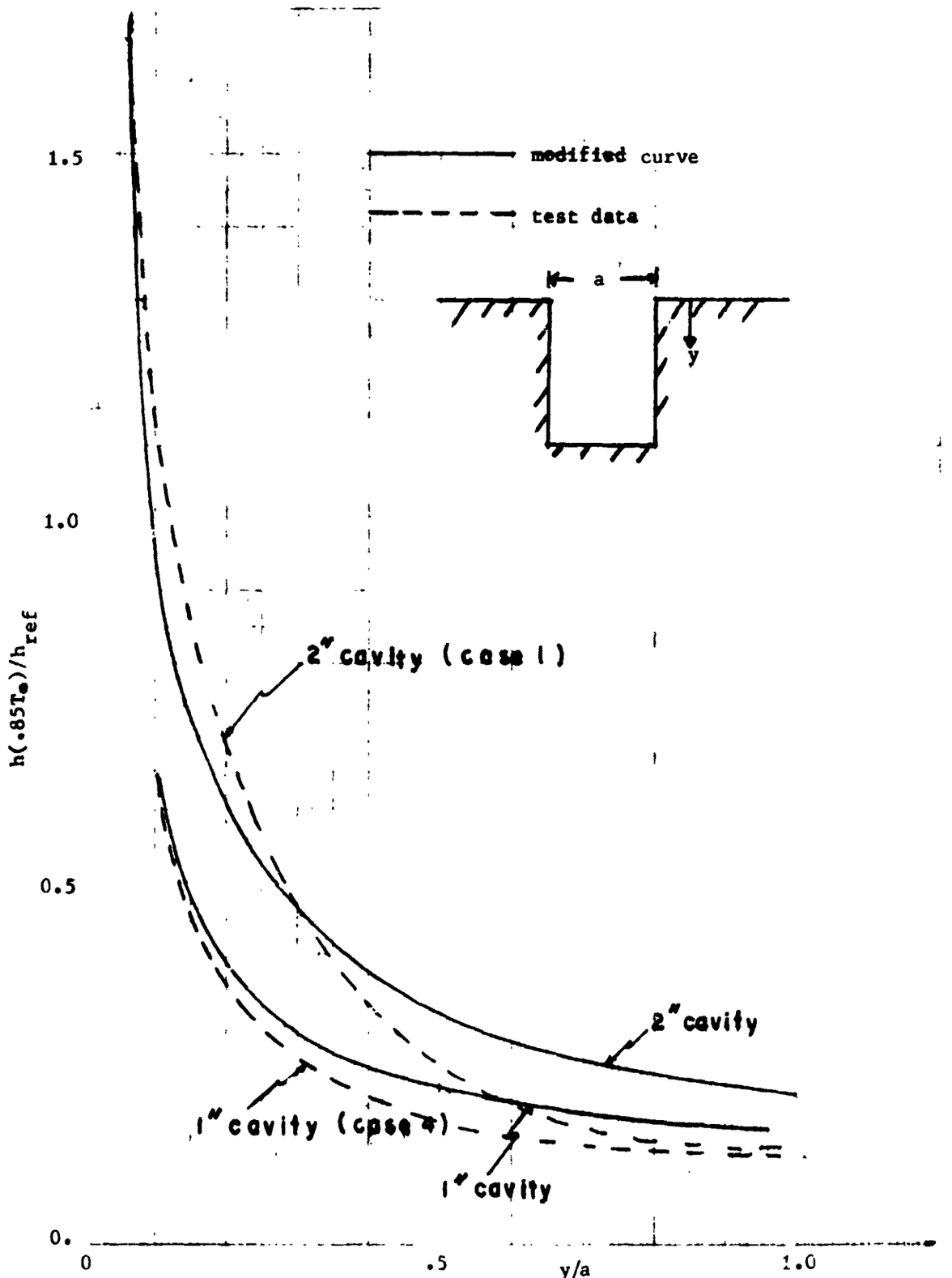

Fig. 25. Comparison between modified Hodgson's theı and test data for zero incidence cases

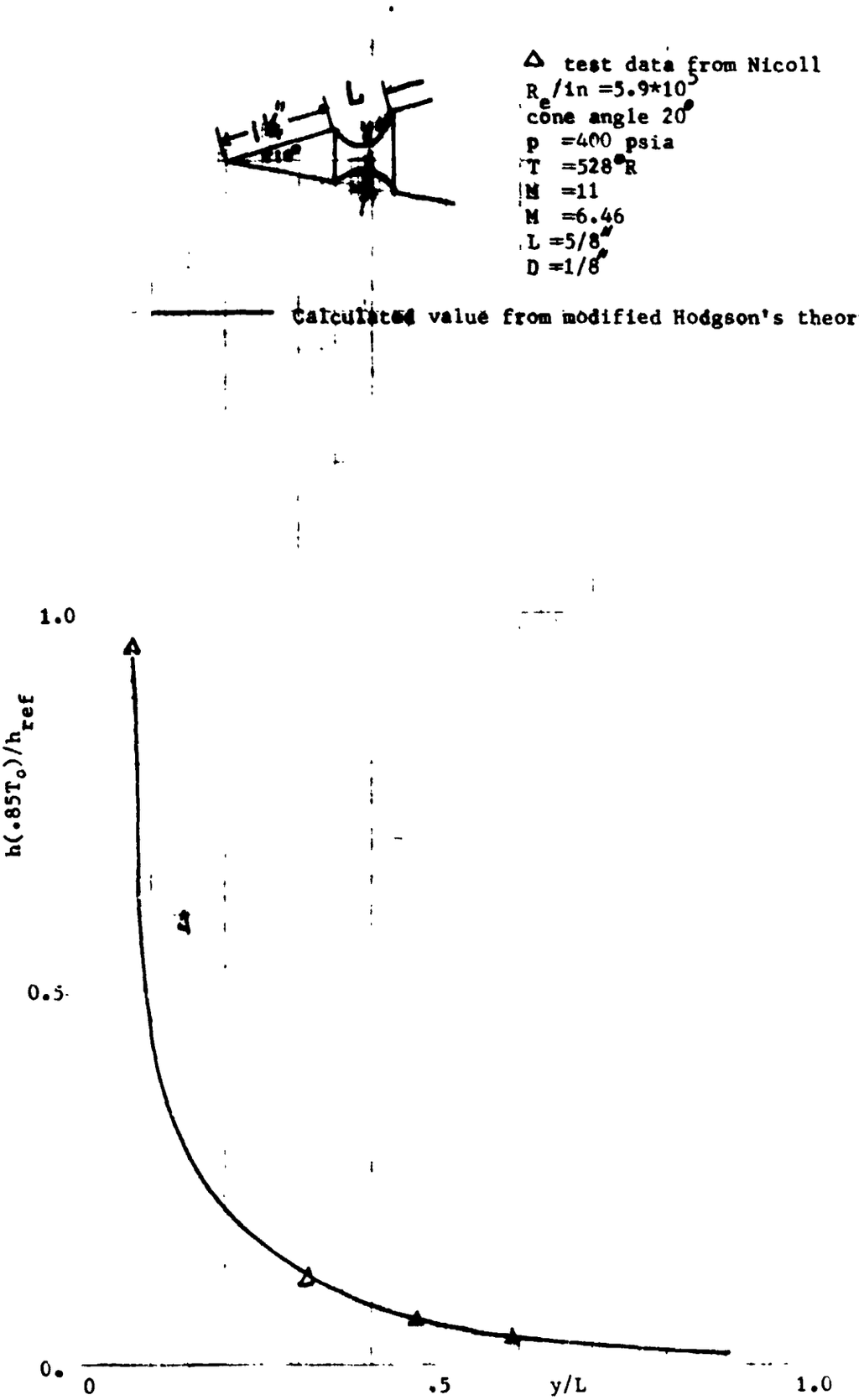

Fig. 26. Comparison between Modified Hodgson's theory and test data in cone-ring case

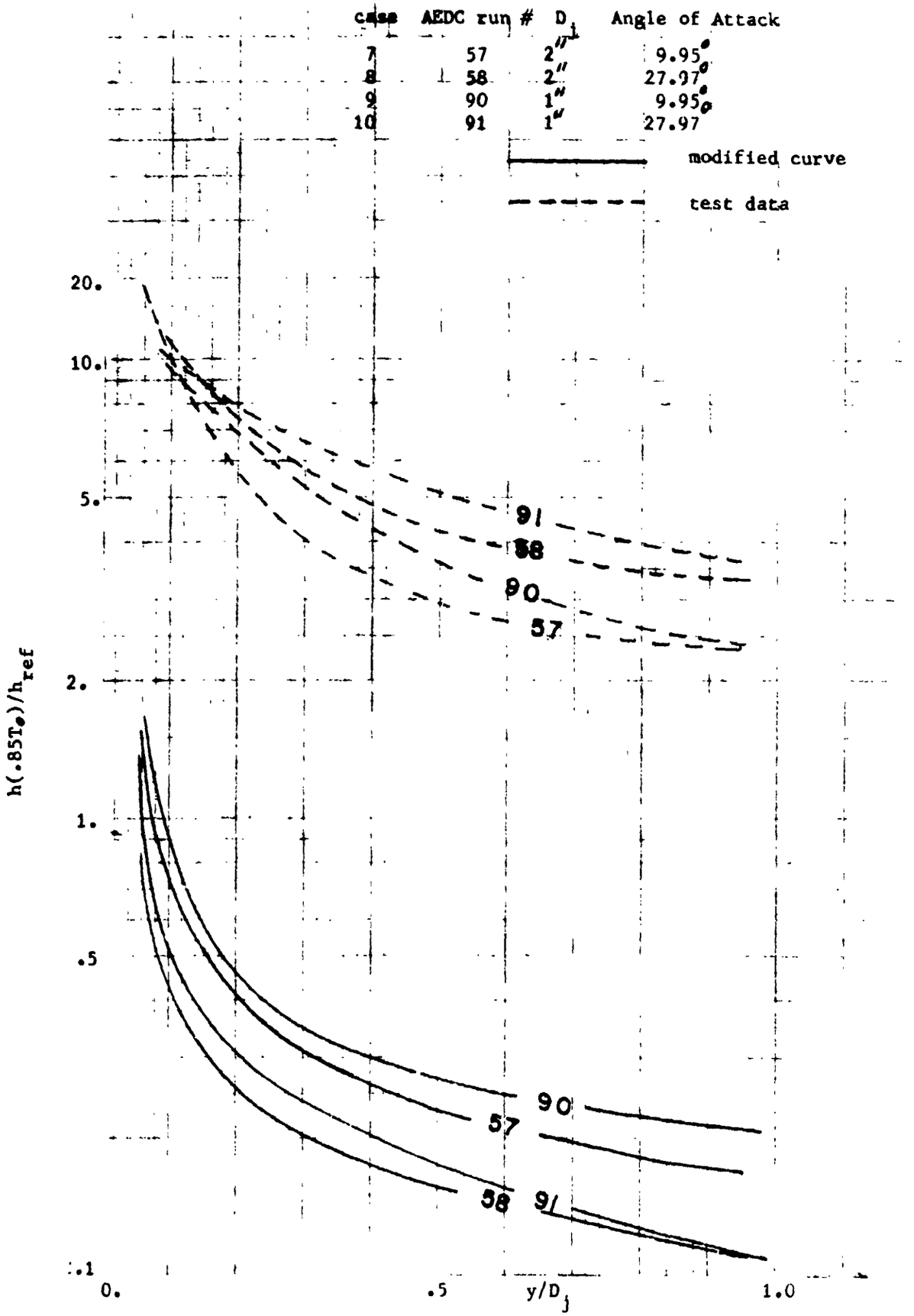

Fig. 27. Comparison between Hodgson's theory and test data with angle of attack

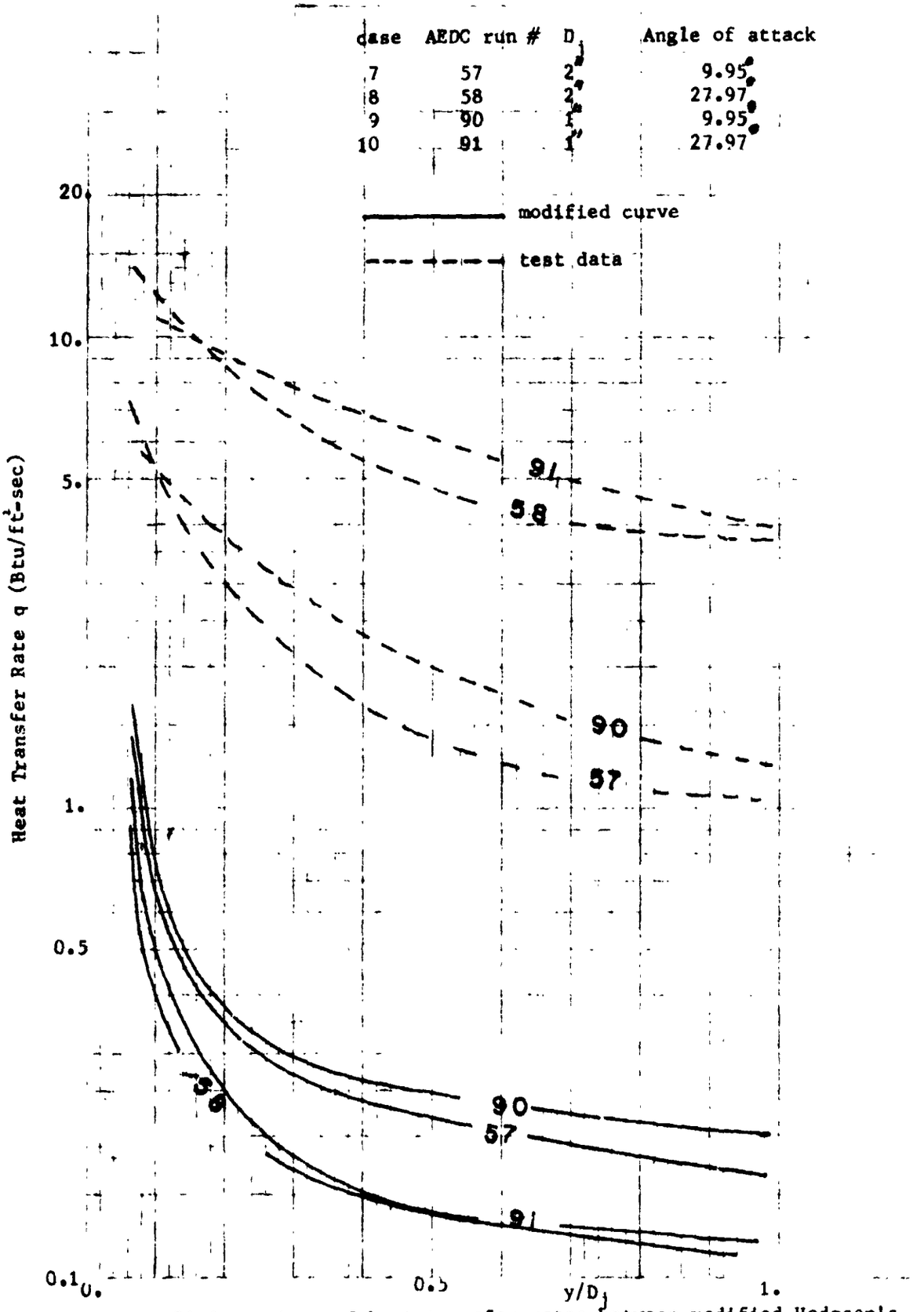

Fig. 28 Comparison of heat transfer rates between modified Hodgson's theory and test data for angle of attack cases

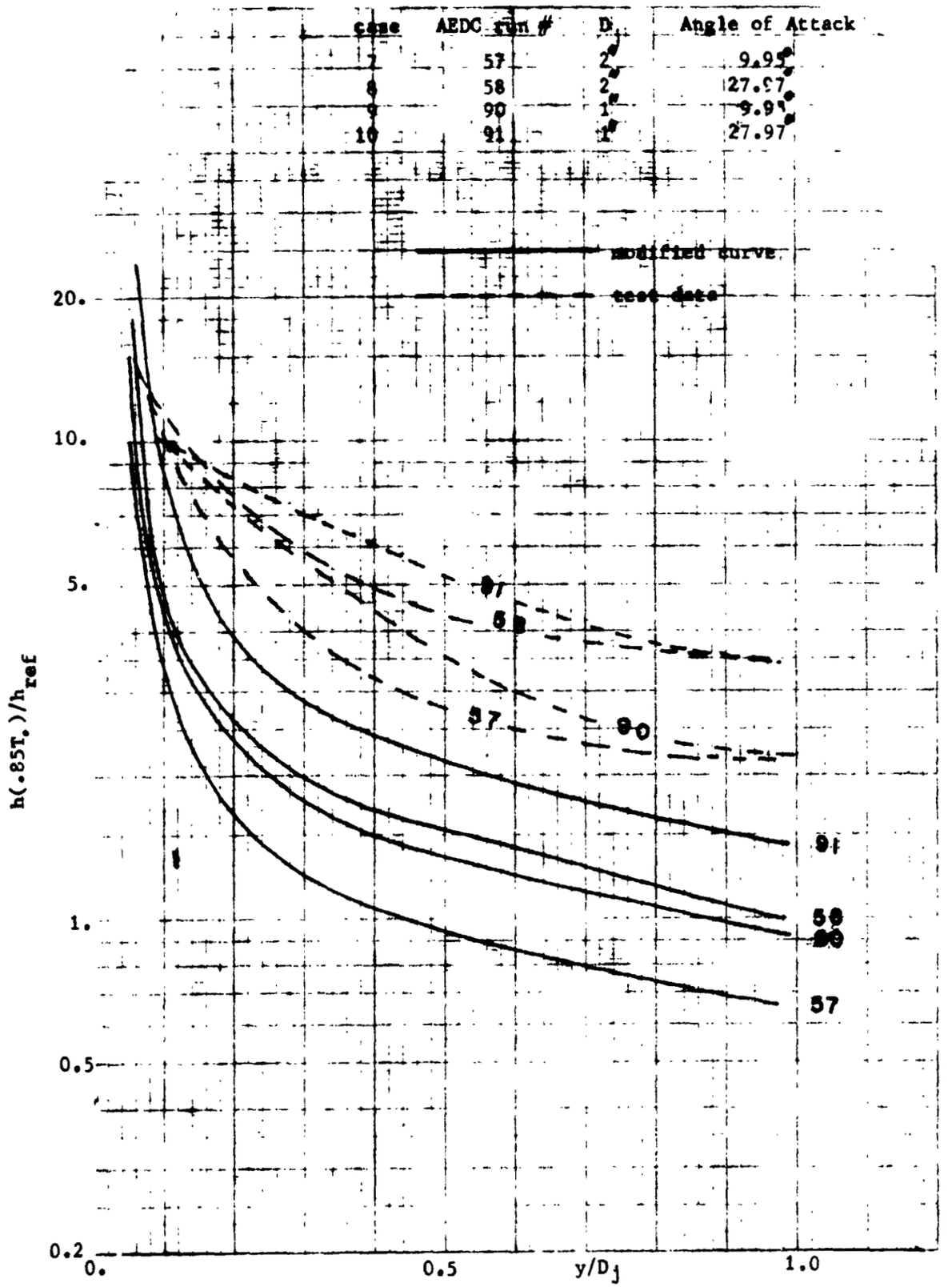

Fig. 29 Comparison between Modified Hodgson's Theory (with increased dividing streamline velocity) and test data for angle of attack cases

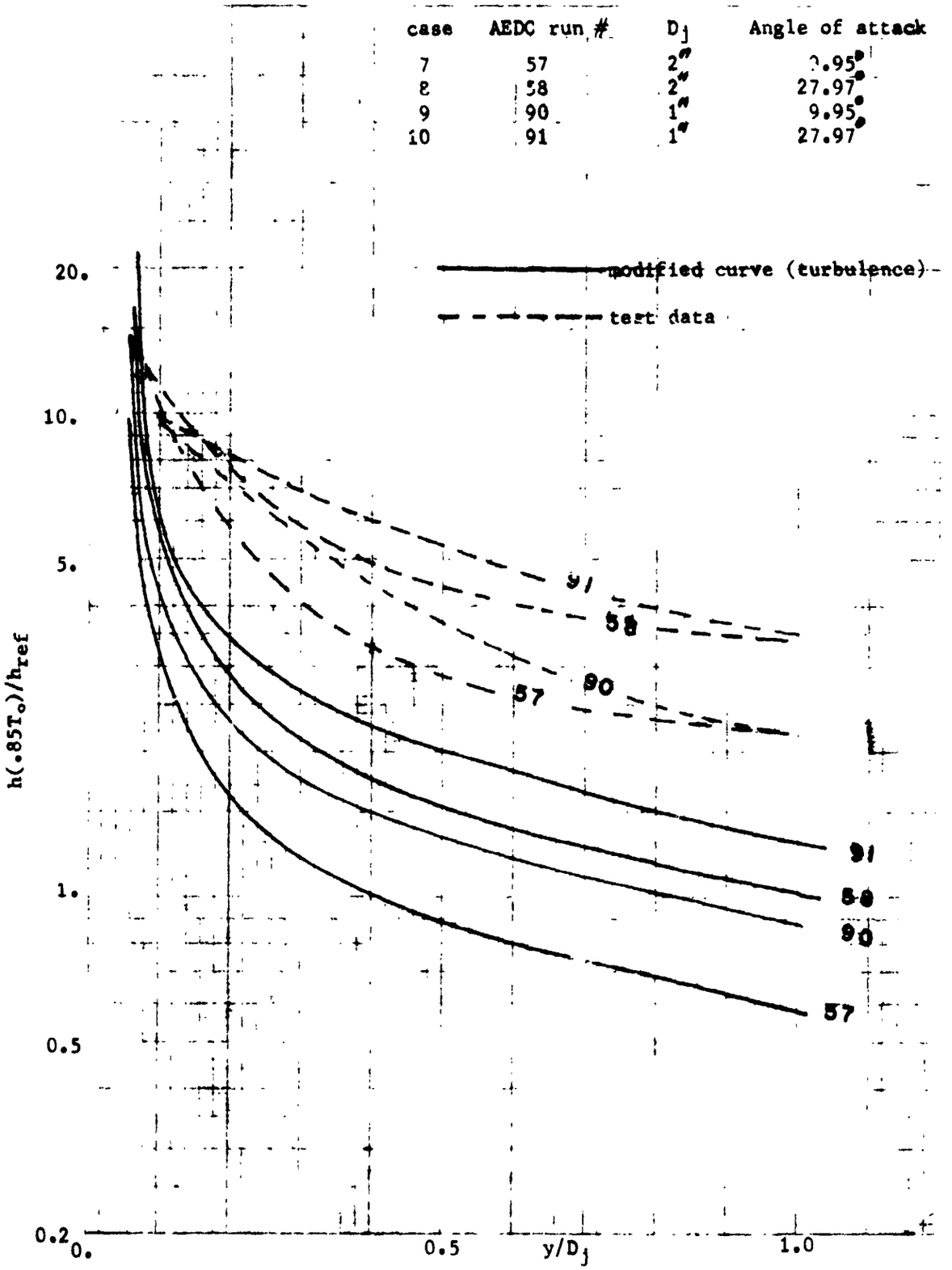

Fig. 30. Comparison between modified Hodgson's theory (with dividing streamline velocity based on turbulent shear layer)and test da for angle of attack cases